INDIUM COMPLEXES AND THEIR ROLE IN THE RING-OPENING POLYMERIZATION OF LACTIDE

by

AMY FRANCES DOUGLAS

B.Sc., The University of Victoria, 2005

A THESIS SUBMITTED IN PARTIAL FULFILLMENT OF
THE REQUIREMENTS FOR THE DEGREE OF

MASTER OF SCIENCE

in

THE FACULTY OF GRADUATE STUDIES

(Chemistry)

THE UNIVERSITY OF BRITISH COLUMBIA

(Vancouver)

April 2008

ABSTRACT

The synthesis and characterization of a series of chiral indium complexes bearing a tridentate NNO ligand are reported. The ligand 2-[[[(dimethylamino)cyclohexyl]amino]methyl]-4,6-bis(tert-butyl) phenol (H_2NNO) was synthesized via a previously published procedure and bound to indium by both a protonolysis and salt metathesis route. A dimethylated indium complex (NNO)$InMe_2$ (**1**) was isolated by reaction of $InMe_3$ with H_2NNO. A one-pot salt metathesis route was used to produce a unique mixed-bridge dinuclear indium complex $[(NNO)InCl]_2(\mu\text{-}OEt)(\mu\text{-}Cl)$ (**3**) from a mixture of indium trichloride, potassium ethoxide and the monopotassiated salt of the ligand, KH(NNO). Direct reaction of KH(NNO) and indium trichloride resulted in the formation of (NNO)$InCl_2$ (**4**) which was carried forward to **3** by reaction with sodium ethoxide.

The complex **3** is active for the ROP of β-butyrolactone ε-caprolactone and lactide and is the first reported indium-based catalyst for lactide or β-butyrolactone ROP. Kinetic studies of **3** for ROP of LA revealed that catalyst was well-behaved, and that the rate was first order with regard to lactide and catalyst. The enthalpy and entropy of activation for the ROP were experimentally determined. Polymer produced by ROP by **3** has narrow molecular weight distribution and a good correlation is seen between the observed moleular weight and monomer loading. A mechanism was proposed for **3** acting as a catalyst for the ROP of lactide; however further experiments are required to confirm this mechanism. Polymer samples isolated from the ROP of *rac*-lactide by *rac*-**3** show isotactic enrichment. It is postulated that the chiral catalyst **3** is exerting stereocontrol via an enantiomorphic site control mechanism.

TABLE OF CONTENTS

LIST OF TABLES

LIST OF FIGURES

LIST OF FIGURES CONTINUED

LIST OF CHARTS

LIST OF SCHEMES

LIST OF ABBREVIATIONS

Anal.	Analysis
br	broad
BINAP	2,2'-bis(diphenylphosphino)-1,1'-binaphthyl
Bn	benzyl, -$CH_2(C_6H_5)$
i-Bu	*iso*-butyl, -$CH_2CH(CH_3)_2$
n-Bu	*n*-butyl, -$CH_2CH_2CH_2CH_3$
t-Bu	*tert*-butyl, -CMe_3
BuLi	*n*-butyllithium
Calc'd	calculated
COSY	Correlated Spectroscopy
d	doublet
deg, (°)	degree(s)
DEPT	Distortionless Enhancement by Polarization Transfer
DMAP	4-Dimethylaminopyridine
ESI	Electrospray Ionization
equiv	equivalent(s)
eq	equation(s)
fac	*facial*
EI	Electron Impact
Et	ethyl
g	grams
GPC	Gel Permeation Chromatography
h	hour(s)
h	Planck's constant
$^1H\{^1H\}$	homonuclear decoupled proton
HETCOR	Heteronuclear Correlated Spectroscopy

H_2NNO	2-[[[(dimethylamino)cyclohexyl]amino]methyl]-4,6-bis(tert-butyl)phenol
HRMS	High Resolution Mass Spectrometry
ITO	Indium tin oxide
J	coupling constant in Hertz
k_b	Boltzmann's constant
k_{obs}	observed rate constant for polymerization reactions
K	equilibrium constant
LA	Lactide
LED	Light emitting diode
LRMS	Low Resolution Mass Spectrometry
m	multiplet(s)
MALDI-TOF	Matrix Assisted Laser Desorption-Time of Flight
M_n	number average molecular weight
M_w	weight average molecular weight
Me	methyl
MeLi	methyllithium
Mes	mesityl, 2,4,6-trimethylphenyl
mer	*meridional*
MWD	molecular weight distribution
MS	mass spectroscopy
NaO^tBu	sodium-*t*-butoxide
NOESY	Nuclear Overhause Enhancement Spectroscopy
NHC	N-Heterocyclic Carbene
NMR	nuclear magnetic resonance
NNO^-	monodeprotonated H_2NNO
NNO^{2-}	doubly-deprotonated H_2NNO
obs	observed
ORTEP	Oak Ridge Thermal Ellipsoid Plot

OTf	triflate, $CF_3SO_3^-$
PDI	Polydispersity Index
Ph	phenyl
pK_a	negative logarithm of the acid dissociation constant (K_a)
PLA	Poly(Lactic Acid)
P_m	Probability of forming a meso linkage
ppm	parts per million
PPY	4-pyrrolidinopyridine
Pr	Probability of forming a racemic linkage
i-Pr	*iso*-propyl, -$CHMe_2$
n-Pr	*n*-propyl, -$CH_2CH_2CH_3$
py	pyridine
q	quartet
R	Universal gas constant
rac	racemic
ROP	ring-opening polymerization
s	singlet
t	triplet
TBD	Triazabicyclodecene
THF	tetrahydrofuran
TMB	1,3,5-trimethoxybenzene
TMS	trimethylsilyl
δ	chemical shift downfield from tetramethylsilane in ppm

ACKNOWLEDGMENTS

I would like to take this opportunity to thank a number of people who made this work possible. Thank you to my supervisor Parisa Mehrkhodavandi for her support and enthusiasm for this work. Thank you to the past and present members of the Mehrkhodavandi Group. I want to especially thank both Insun Yu and Jennifer Fang. Insun for growing crystals of the (NNO)$InMe_2$ complex and Jennifer for her tireless work in setting-up the lab. Thank you to the Gates group, especially Bronwyn Gillon and Kevin Noonan, for the use of their GPC instrument and the time they spent helping me figure out how to use it.

Thank you to the all the UBC Chemistry Department staff, especially Brian Snapkauskas and the mech shop guys who always found time to fix the numerous problems we had in setting up a new lab. A particular thank you should go to Brian Patrick for solving the crystal structures that are contained in this work. Especially for the extra time he took to solve the data for the structure of the catalyst. I would like to thank the NMR staff Nick Burlinson, Maria Ezhova and Zorana Danilovic for their help with both the kinetic studies and the homonuclear decoupled NMR.

Thank you to my family (my parents John and Frieda, and sisters Carole and Lauren) for your faith in my abilities, and the endless support. Last, but not least, I'd like to thank Tim for taking a chance and asking "Do you want to grab a cup of coffee?" I couldn't have done this without you (or the coffee).

CHAPTER 1. GENERAL INTRODUCTION

1.1 Introduction to Poly(Lactic acid)

In recent years biodegradable polymers and polymers from biorenewable resources have received a great deal of attention as alternatives to traditional petrochemical based polymers. In particular poly(lactic acid) (PLA) has received a large amount of industrial interest (Chart 1.1). Cargill-Dow LLC and other companies have developed the infrastructure for both the manufacture and processing of PLA.[1] This has caused a significant drop in the cost of the plastic and has led to an increased use of PLA in a number of applications such as the textile industry, the packaging industry for both food and horticultural applications, and in the pharmaceutical and biotechnology industries.[2]

Chart 1.1. Molecular structure of poly(lactic acid)

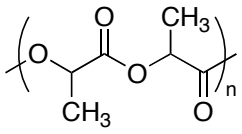

Poly(lactic acid)
PLA

PLA's many applications stem from its biodegradability and bioassimilability. Current industrial uses for PLA include its use in "green" disposable packages in the food and beverage industry. Under suitable conditions such as composting the plastic containers will degrade to carbon dioxide and water, preventing the plastic from entering the traditional waste streams. PLA has been used in the medical industry for many years; one of its first applications was in

sutures for surgical procedures (a composite of PLA and poly(glycolic acid) is used). The sutures need not be removed and are gradually degraded by the body's natural pathways. Similarly, screws made of PLA are used for the fixation of bones or joints. Because the screws degrade over time, secondary surgeries are not required in order to remove the unnecessary hardware after the desired healing process has been achieved.

Current research, both industrial and academic, has focused on using PLA in controlled drug delivery by biodegradable devices. The drug is encapsulated in a polymer matrix that is implanted subcutaneously; the active drug is slowly and continually released over time as the polymer is degraded. Alternatively, nano or microparticles of drug-encapsulating polymers have also been explored for use in drugs administered either orally or nasally. In this case the polymer formulation might allow for more specific targeting of the drug to a particular active site.

PLA microstructure has a strong influence on the polymer properties. There are a number of possible microstructures for PLA due to the different ways of incorporating the isomers of lactide (LA) (Chart 1.2) into the polymer chain. Poly(L-lactic acid) (PLLA), and poly(D-lactic acid) (PDLA) are both crystalline polymers with melting points of 180 ºC, while atactic PLA produced from the polymerization of DL-lactide is an amorphous polymer with a melting point of 130 ºC. Stereocomplexes of PLA, a physical mixture of PLLA and PDLA, can have even higher melting points at 210 ºC. The processing methods for these polymers can also influence their properties.

Chart 1.2. Isomers of lactide generated from DL-lactic acid.

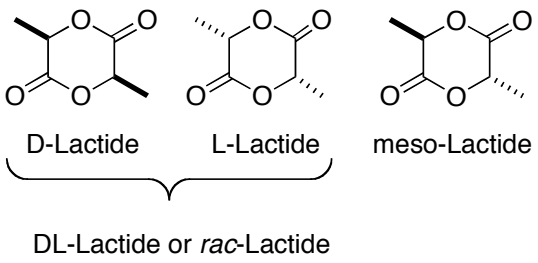

Degradation of PLA occurs through two mechanisms: hydrolysis of the polyester chain, and enzymatic degradation. Acidic or basic conditions can be used to catalyze the hydrolysis; elevating both the temperature and humidity increases the hydrolysis rate. The rate of hydrolysis is dependent on a number of factors, including the molecular weight and the crystallinity of the polymer. Once the polymer has been hydrolyzed into small oligomeric chains (< 40 000 g mol^{-1}) bacteria and other microorganisms can further degrade the polymer to carbon dioxide and water via the Kreb's cycle. Although PLA degrades relatively easily when compared to traditional plastics, further research into the infrastructure required for large-scale degradation of the plastic, as well as for monomer recovery/recycling is required. To that end, research has begun in order to find enzymes suitable for degrading PLA.

Lipases, such as proteinase K, are active in the biodegradation of PLA. Proteinase K is very efficient at breaking down PLA; however, it is not active for the degradation of high molecular weight PLA. A two-step degradation pathway involving both hydrolysis and enzymatic digestion of the polymer is required for high molecular weight PLA.[1] Recently enzymes from a yeast *Cryptococcus* have been isolated and used to degrade high molecular weight PLA, as well as other biodegradable polymers such as poly(caprolactone).[3] It has been shown that enzymes have a strong preference for the degradation of PLLA versus PDLA. The

highest rates were observed for the degradation of the amorphous regions in samples of PLA that contained atactic PLA.[4] Further research is required into the degradability of other microstructures of PLA.

Achieving control over polymer formulations and microstructures is often accomplished by using a living catalyst. As defined by the IUPAC Compendium of Chemical Terminology, a living polymerization is "A chain polymerization from which chain transfer and chain termination are absent. In many cases, the rate of chain initiation is fast compared with the rate of chain propagation, so that the number of kinetic-chain carriers is essentially constant throughout the polymerization."[5] If a polymerization is truly living, and follows these criteria, the molecular weight distribution of the polymer chains is uniform, and the rate of consumption of monomer is constant throughout the polymerization. It also follows that the molecular weight of the polymer will increase linearly with conversion until one hundred percent conversion is achieved. If no termination processes are present in the system, it is possible to restart the polymerization after complete conversion via addition of more monomer.

There are several measureable characteristics for a living polymerization. The narrow molecular weight distribution (MWD) can be determined by the measurement of the molecular weights of the polymer chains. MWD or polydispersity index (PDI) is defined as the weight average molecular weight divided by the number average molecular weight (M_w/M_n). Both the M_w and the M_n can be determined by gel permeation chromatography or GPC. GPC can also be used in conversion experiments to determine the molecular weights of polymer samples. The rate of consumption of monomer is usually demonstrated through kinetic experiments.

Transesterification is the major chain transfer mechanism in the polymerization of LA (Scheme 1.1).[6] For intermolecular transesterification two growing polymer chains come together

and a random exchange of polymer ends occurs. This leads to a scrambling in the molecular weights observed for the polymers, and a broadening of the PDI. Alternatively the transesterification can occur through an intramolecular process causing the formation of cyclic polymers.[7] In the case of both inter- and intra- transesterification, lactate subunits from the cleavage of a lactide unit can be identified by MALDI-TOF (matrix assisted laser desorption ionization-time of flight) mass spectrometry.[8] Chain termination processes for polymerization usually result from decomposition of the catalyst, or by introduction of a proton source, such as water, into the reaction mixture.

Scheme 1.1: Transesterification mechanism for the polymerization of lactide (both intramolecular and intermolecular).

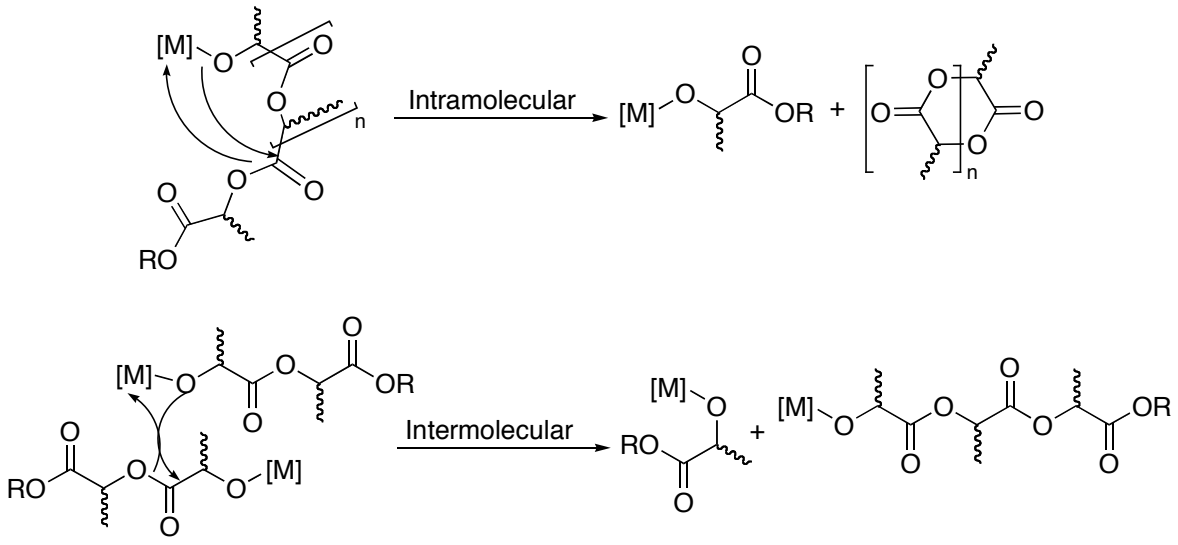

If the chain transfer and termination mechanisms can be prevented, the system is living. A living system is desirable because it allows for precise control of polymer molecular weight via control of catalyst loadings and reaction times. Polymer compositions can be controlled through copolymerizations of different monomers; block copolymers can be formed

via control of the monomer feedstock. Due to this precise control, developing living systems is one of the major goals in polymer research. One area of success in this field is in the development of new organometallic complexes as catalysts for the polymerization of olefins. This has led to an increased knowledge base in the area of catalyst and ligand design, as well as a huge increase in research into developing new catalyst systems. In the body of this work the development of a catalyst for the living polymerization of lactide will be discussed.

1.2 Synthesis of PLA Industrially

PLA can be synthesized directly from the condensation of lactic acid. Lactic acid is produced commercially by fermentation of food-crops or from petrochemical feedstocks. Biological based lactic acid is exclusively the L-isomer (Scheme 1.2) as it is fermented from the naturally occurring sugars. In contrast petrochemical based lactic acid is a racemic mixture of D- and L-lactic acid, and is prepared by the oxidation and functionalization of ethylene.[2] In recent years the fermentation process has become more cost effective and it is now the favored method for producing lactic acid. Since lactic acid can be isolated by the fermentation of crops such as corn or other vegetation, it is considered a biorenewable feedstock.

Scheme 1.2: The isomers of lactic acid and its direct condensation to form PLA

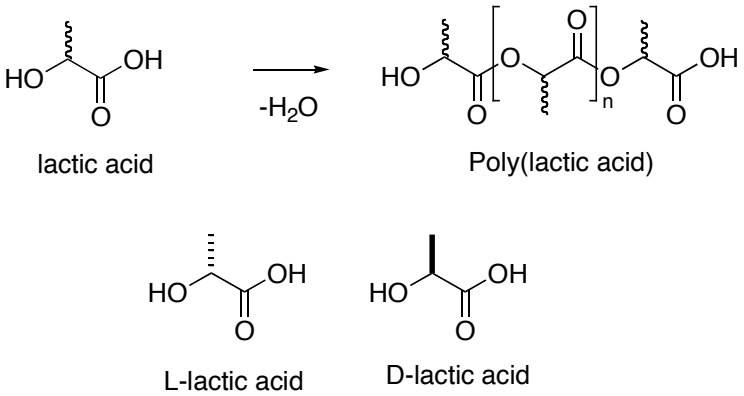

One industrial route to PLA has been developed by Mitsui Toatsu Chemicals. They have optimized, and patented an azeotropic dehydrative process that uses a condensation route to produce PLA.[1] This process uses high temperatures and high boiling solvents in order to remove water and drive the polymerization through to completion producing high molecular weight polymers.

The second industrial route to PLA, used by Cargill-Dow LLC involves metal-based ring-opening polymerization of lactide (LA), and is outlined in Scheme 1.3.[1] Lactic acid undergoes a condensation to form low molecular weight prepolymer. The prepolymer is then depolymerized using a tin based metal catalyst to produce lactide. After purification by distillation, the lactide undergoes ring-opening polymerization (ROP) catalyzed by a different tin catalyst to form high molecular weight PLA. There are several advantages to this polymerization method. No solvents are used as all processes are carried out in the melt (m.p. of lactide is 116-119 ºC). This makes the Cargill-Dow process a green alternative to the solvent-based process used by Mitsui Toatsu Chemicals. The metal-based catalysis allows for good control over

polymer properties such as molecular weight. Since Cargill-Dow uses biologically synthesized lactic acid, the polymer produced by this technique is almost exclusively poly(L-lactic acid).

Scheme 1.3: Metal-based industrial preparation of PLA.

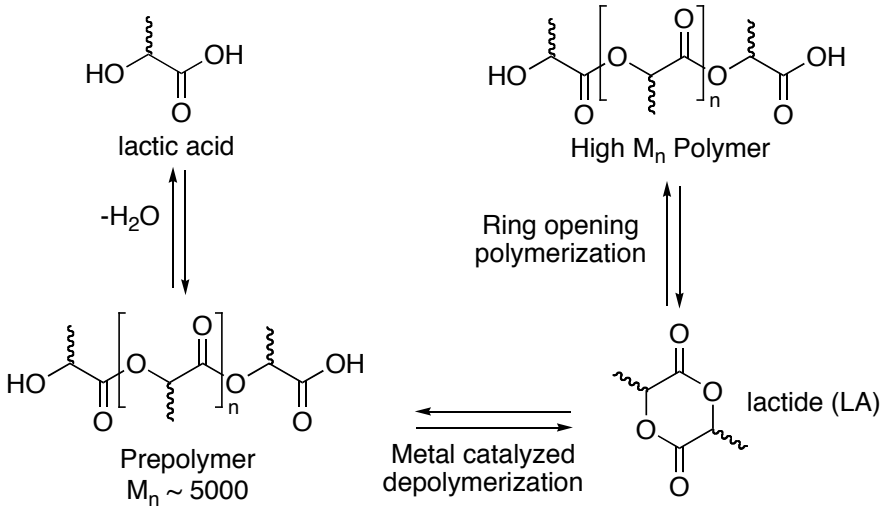

1.3 Ring-opening polymerization of LA

The industrial routes to synthesize PLA are not the only possible routes to formation of PLA; there are many routes to ROP lactide including enzymatic, anionic, cationic, organocatalytic, and metal catalyzed polymerizations.[9] The ring-opening process is favorable in all of these cases due to relief of a larger than normal ring-strain for lactide when compared to other six-membered rings. In this case the high degree of ring-strain is due to the unusual geometric conformation imposed on the ring by the presence of the two ester groups in the ring.[10] The ester groups are nearly planar forcing the ring into an irregular skew-boat conformation with the methine protons at the axial and the methyl substituents at the equatorial positions of the structure. The ring-opening of the strained lactide drives the polymerization; standard enthalpy

of polymerization is −23 kJ mol^{-1} and standard entropy of polymerization is −40 J K^{-1} mol^{-1} for the formation of poly(L-lactic acid). The negative entropic value indicates a critical temperature, calculated to be 557 K (a value of 913K was obtained for polymerizations carried out in the bulk), at which the polymerization will become non-spontaneous. [11]

The enzymatic route for the ring-opening polymerization of lactide uses lipases to catalyze the polymerization.[12-14] Using an enzyme to catalyze the polymerization circumvents the need for purification of the polymer in order to remove metallic catalysts, which is necessary if the polymer is to be used for medical or food packaging applications. Most lipases that are effective in catalyzing the ROP of LA produce high molecular weight polymers with small values for the polydispersity index (1.1-1.2). Lipase PS produces polymer with the highest conversion rate and molecular weights. Lipase catalyzed polymerizations are carried out in the melt, avoiding the use of organic solvents; however, the polymerizations require lengthy reaction times (7-14 days) at elevated temperatures (80–130 ºC).[13] More recently, the use of this route along with multifunctional alcohols has produced branched polymers of lactide. Branched PLA differs from linear PLA in its thermal, physical and mechanical properties. It has also been shown that branching increases the rate at which PLA is degraded by both enzymatic degradation and base hydrolysis. [12]

Anionic polymerization of lactide was one of the earlier methods developed for the controlled polymerization of lactide. Starting with the pioneering work of Kricheldorf in the late 1980's and 1990's it was discovered that strong bases such as alkyl lithium reagents and highly basic alkoxides were active for the polymerization of lactide at room temperature.[6,15] Two mechanisms were proposed (Scheme 1.4). The first involves deprotonation of the monomer. The methine proton is removed from the lactide, forming an enolate type structure, which can then

ring open. The remaining anionic chain acts as a propagating species and continues the polymerization. The second mechanism involves nucleophilic attack by the base on lactide and subsequent ring opening of the monomer. In this case initiator fragments would be incorporated as chain ends in the growing chain. This is not observed for initiators such as n-butyl lithium or potassium tert-butoxide. The easily identifiable tert-butyl ester end-group is not observable by ^{1}H NMR spectroscopy and in the case of the butyl reagent the evolution of butane is observed. This evidence supports the deprotonation route for the polymerization of lactide by anionic initiators.

Scheme 1.4: Proposed mechanisms for the anionic ring-opening of lactide

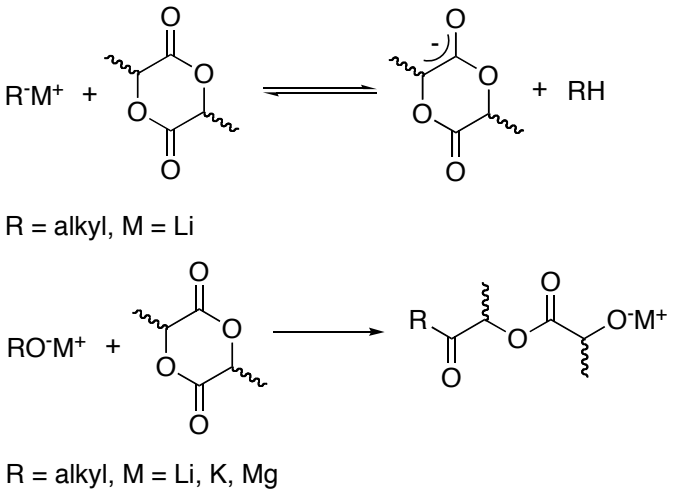

Competitive processes occur during anionic polymerization. The polymerizations are low yielding, and the correlation between observed molecular weight versus monomer to initiator ratio is non-linear. As the polymerization proceeds, the polydispersity of the polymer samples increases. This is an indication that transesterification is occurring during polymerization. For anionic polymerizations, this process is more prevalent at longer reaction times and elevated temperatures.

Racemization of the lactide monomer is a phenomenon observed during anionic polymerization of lactide.[6] It has been shown that for both strong and relatively weak bases can cause racemization of the monomer. As shown by the deprotonation mechanism for anionic polymerization (Scheme 1.4), an equilibrium exists between the protonated and deprotonated monomer, which allows for scrambling of the stereogenic centre. In the polymerization of L-lactide, racemization of the monomer occurs throughout the polymerization and it increases with longer reaction times as observed by the optical rotation of polarized light by the polymer samples isolated at different times. This indicates that the chain ends also play a role in the racemization of the monomer. An increase in reaction temperature also leads to an increase in the scrambling of the stereocentres. Lower temperatures and initiator loadings can minimize the amount of racemization, although these limitations consequently increase the reaction times.

Cationic polymerization of lactide has also been explored. Kricheldorf laid down the groundwork in the field with his investigation of methanesulfonic acid and methyl triflate as catalysts for the ring-opening polymerization of lactide.[16] He found that the cationic catalyst could readily polymerize lactide, with no epimerization of monomer stereocentres. He also found that the counter anion for the polymerization played an important role in whether the cation would polymerize lactide. Simple Lewis acids such as BF_3•OEt_2, or zinc fluoride were not successful as catalysts, and neither were a variety of organic acids (trifluoroacetic acid, methanesulfonic acid, and fluorosulfonic acid). A number of alkyl sulfonates were tried as catalysts of these methyl triflate was the only active catalyst.[17] The reactions required several days at room temperature in order to reach completion, and if the temperature was elevated above 50 ºC racemization of the monomer became an issue. Another critical problem with the cationic approach was lack in correlation between polymer molecular weight and the initial catalyst loading; the relative viscosities of the polymer samples showed no significant

difference for samples made from different catalyst loadings. These results indicate a severe limitation in the use of cationic catalysts for the polymerization of lactide.

The proposed mechanism for the cationic polymerization of LA follows an activated monomer route Scheme 1.5. In this case the acid activates the carbonyl of the monomer making it susceptible to nucleophilic attack. The ring is opened via cleavage of the acyl bond. This ring-opened product can then act as the nucleophile for propagation of the polymerization.[16]

Scheme 1.5: Proposed mechanism for the cationic ring-opening of lactide

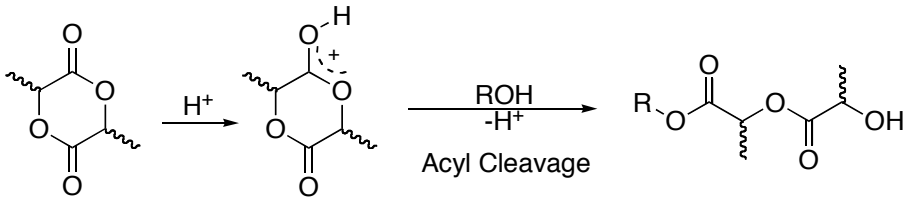

More recently the scope of cationic polymerization has been expanded to lactone monomers other than lactide. Both ε-caprolactone and γ-valerolactone were polymerized by combining HCl and an alcohol (butanol and more complex multifunctional alcohols).[18, 19] The polymer samples displayed narrow molecular weight distributions and high yields of polymer for short reaction times; furthermore, adjustment of the monomer to initiator ratio controlled the molecular weight of the polymers. The catalyst system was also used to produce block copolymers of the two monomers. Considering the simplicity of the reagents for catalysis, the cationic route to synthesizing polyesters seems highly desirable; however, several limitations still exist. Lactide is less readily polymerized than either caprolactone or valerolactone. To address this, Bourissou and co-workers re-examined the earlier work carried out by Kricheldorf,

and optimized his system for the polymerization of lactide.

Bourissou's group uses a combination of a protic reagent such as simple alcohol and trifluoromethanesulfonic acid in order to polymerize lactide.[20] This differs from the work carried out by Kricheldorf. In Kricheldorf's case he did not add a secondary protic agent as a co-catalyst. The system gives polymer samples with high conversions, low molecular weight distributions (PDI < 1.5), short reaction times (< 4h for 125 equivalents) and a linear relationship is observed between molecular weight and catalyst loadings. By ^{1}H NMR analysis of the polymers it can be seen that the end groups for the polymer are consistent with acyl-bond cleavage; namely, both ester and hydroxyl chain ends were observed.

Another rapidly expanding area in the polymerization of lactide is in the use of organocatalysts. Where an organocatalyst is defined as an organic compound that in the absence of a metal species acts as a catalyst for a given reaction. Both pyridine-based nucleophiles, and N-heterocyclic carbenes (NHCs) have demonstrated activity in the ring-opening polymerization of lactide (Chart 1.2).[8, 21-24] All of the organocatalytic catalysts have the characteristics of a living system; they show narrow MWD, linear conversion of monomer to polymer, and a good correlation between the molecular weight of the polymers and the monomer to initiator ratios.

Chart 1.3: Organocatalytic reagents for the polymerization of lactide

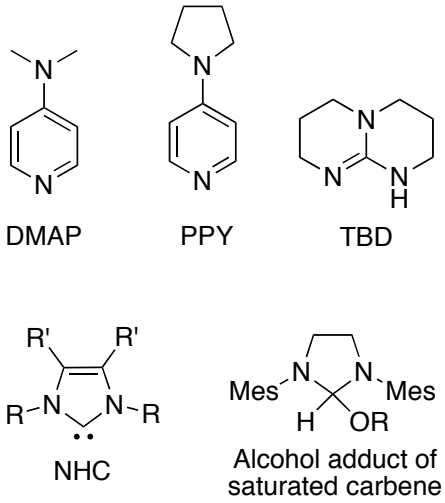

The polymerization mechanism for the organocatalysis follows an activated monomer pathway (Scheme 1.6).[24] The first step in the mechanism is the formation of a base-lactide complex by attack of the carbonyl of the monomer by the strong organic nucleophile. The nucleophilic attack causes the lactide ring to open via an acyl bond cleavage. The lactide-base complex then undergoes nucleophilic attack by either the original alcohol initiator or by the terminal ω-hydroxy group on the end of a growing polymer chain, releasing the original organocatalyst. The chain is propagated by further nucleophilic attack of the chain end ω-hydroxy group on activated lactide monomers.

Scheme 1.6. Mechanism for polymerization of LA by nucleophilic activation of the monomer

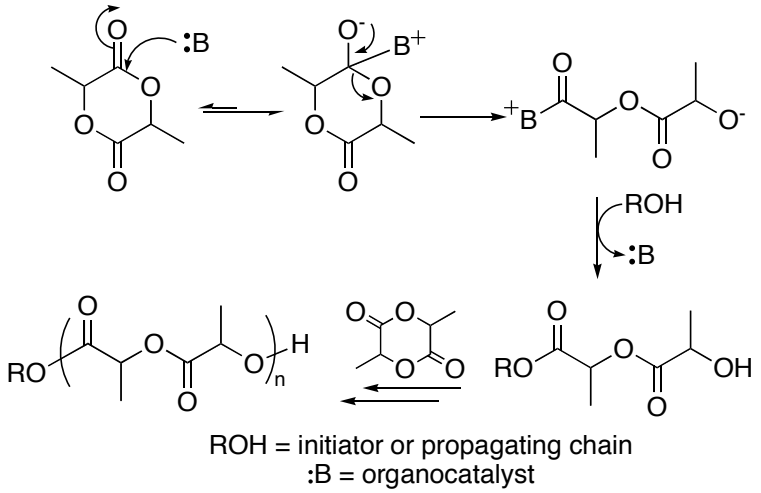

If an initiator and a carbene are used in the polymerization of LA, linear PLA is produced.[22, 23] Either an alcohol can be added to the reaction mixture or a masked carbene (in Chart 1.2 the alcohol adduct of the saturated carbene) can be used. In this case, the masked carbene acts as the source for both the initiator and the base; dissociation of the adduct results in the formation of ROH and the unsaturated carbene.[22] When an initiator is absent from the reaction mixture and the NHCs are used cyclic oligomers or polymers are formed exclusively.[8] In the case of the NHC polymerization in the absence of an initiator a zwitterion is formed upon ring opening, with the positively charged carbene bound to one end of the chain. The chain can propagate by the mechanism outlined above. However, termination of chain growth occurs through a slightly different mechanism. Coulombic forces between the chain ends cause them to come together, releasing the NHC and a cyclic polymer. The NHC can then initiate the growth of a new polymer chain.

The reaction times for polymerization of lactide using carbenes are rapid. In a

representative reaction conversion of 200 equivalents of LA to PLA is achieved in two minutes, making carbenes the most active known catalysts for the polymerization of lactide. Interestingly, the very sterically bulky carbenes also show some degree of stereoselectivity during polymerization.[23]

The final mechanism to be discussed is the metal mediated ring-opening polymerization of lactide. This is perhaps the most widely explored area in the catalysis of LA polymerization. It has been found that a number of metals are capable of polymerizing lactide including magnesium[25-33], calcium,[28, 34-37] yttrium,[38-49] the lanthanides,[50-56] tin,[57-60] iron,[61-64] zinc,[25, 26, 28, 29, 31, 55, 65] aluminum,[7, 25, 40, 55, 66-74] and germanium.[75, 76] Simple metal alkoxides of iron[64], tin,[77]yttrium,[78, 79] the lanthanides,[78, 79] calcium,[80] and aluminum[7] are effective catalysts. Unfortunately the polymers produced from these catalysts have large molecular weight distributions, and analysis by MALDI-TOF MS shows that transesterification is occurring during polymerization. Due to these disadvantages, non-labile ancillary ligands were used in order to introduce steric bulk at the metal centre in the hopes of preventing the deleterious side reactions. A general formula for these catalysts is L_nMR where L_n are ancillary ligands that do not play an active role in the polymerization, but do strongly influence the metal centre and its behaviour in the polymerization. M is a Lewis acidic metal centre, and R is the initiating group. In general the most effective initiator group is an alkoxide, but alkyls, amides, and halides have been found to initiate the polymerization. However, it was not conclusively shown that protic impurities in the monomer such as lactic acid, alcohols or water were not acting as the initiator in these cases.

These metal mediated polymerizations are thought to occur through a coordination insertion mechanism (Scheme 1.7). The first step in the mechanism is coordination of one molecule of lactide to the active metal centre via a dative bond between the oxygen of the

carbonyl and the metal. This is followed by insertion of the monomer into the metal alkoxy bond via a nucleophilic attack at the carbon of the carbonyl by the initiator group (the alkoxy group). The ring is then opened via cleavage of the acyl bond. In the case of an alkoxy initiator this leads to an ester on the polymer chain end, and an alcohol end group if hydrolysis of the catalyst occurs. Experimental evidence for this mechanism was first shown in the late 1980's by the groups of Kricheldorf and Teyssié. [7, 81]

Scheme 1.7: Metal-catalyzed coordination-insertion mechanism for the ROP of LA.

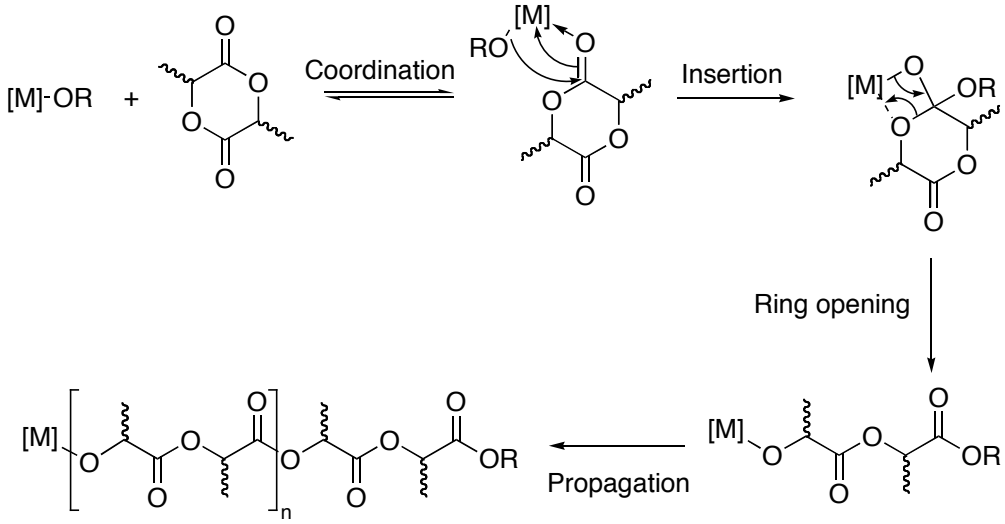

Some of the first ancillary ligand systems developed for the polymerization of lactide were the metalloporphyrin systems synthesized by Inoue and co-workers in the late 1980's (Chart 1.4).[71, 82] These systems gave polymers of narrow molecular weight distribution, in high yield. Polymerization of γ-valerolactone showed that the reaction showed second-order dependence on the catalyst concentration. A mechanism by which two aluminum centres play a role in the polymerization of the monomer was proposed. In this mechanism the initiator group of one catalyst acts as nucleophile in an attack on the carbonyl of the monomer, which is being

activated by the other equivalent of the catalyst. In this case the aluminum centre acts as a Lewis acid to activate the carbonyl of the monomer. The reaction itself is not very rapid (the conversion of 100 equivalents of lactide went to completion after 96 h) and the reaction requires high temperatures (100 ºC) to proceed.

It was postulated that a more flexible ligand might allow for a unimolecular pathway for chain growth, because of the less constrained geometry at the metal centre. The incoming monomer and the initiator have to have a cis-geometry in order for the coordination-insertion mechanism to be viable. In the case of the porphyrinato ligands the metal is completely encompassed by a very rigid equatorial ligand, leaving only two trans axial sites for the coordination of the initiator and the monomer.

To this end, the Bertrand group developed aluminum, zinc, samarium and tin diamidoamino complexes for the polymerization of lactide.[68, 83-85] The complexes of aluminum have trigonal monopyramidal geometry. A similar geometry was seen for the tin analogue while the zinc and samarium complexes were dimeric. The tin system was found to be the most active when bulk copolymerizations with glycolide were attempted. However, the PDI for the polymer samples were large (3 for polymerizations at 180 ºC, and 2 for polymerizations at 140 ºC).

Chart 1.4: Important and common ligand motifs in catalysts for the polymerization of lactide

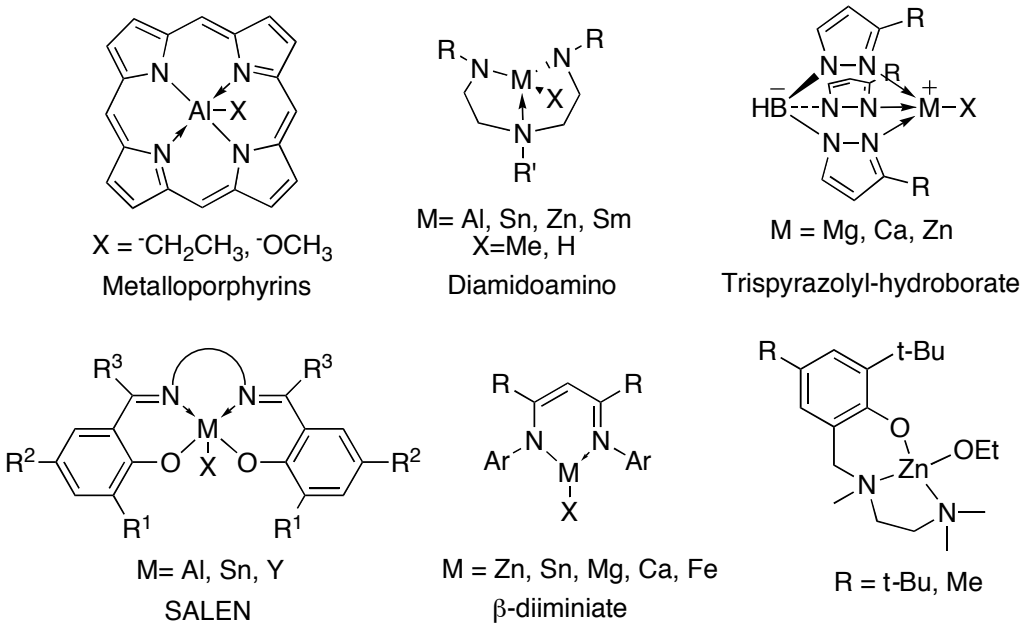

A bulkier tridentate ligand was used to prevent transesterification reactions. The sterically bulky trispyrazolyl-hydroborate ligand was used on magnesium, calcium and zinc to form complexes for the polymerizations of lactide. [26, 28, 30, 34] It was found that the calcium analogue was the most active, with the others falling into the series Ca > Mg > Zn. This was attributed to the polarity of the metal-initiator bond. The calcium analogue could polymerize 100 equivalents of lactide in one minute at room temperature. The trisindazolyl-hydroborate analogues of zinc and magnesium were also synthesized. The change in the ligand caused an increase in the activity of the catalysts. The systems showed a first order dependence for the polymerization upon the concentration of the catalyst, but the PDI values were quite high for the polymer samples (1.6-1.7).

Salen based catalysts have been widely studied for the polymerization of LA. Inspired by the porphyrinato systems of Inoue, the range of salen catalysts includes aluminum, [67, 69, 73, 74, 86]

yttrium,[40] tin,[87] and zinc analogues.[88] Changes in the ligand backbone can play a major role in the activity of the catalyst. It was found that when the backbone is flexible the rate of polymerization is higher than when a rigid backbone is used. [69] Steric bulk at the R^1 position of the ligand (Chart 1.4) slows the rate of polymerization but enhances the stereoselectivity. The polymerizations rates are first-order in catalyst concentration, and the polymer samples contain ester end groups indicating a coordination insertion mechanism with acyl bond cleavage (Scheme 1.7). The polymers have narrow molecular weight distributions and a linear relationship is observed between the conversion and molecular weight, indicating the salen catalysts are living.

The salan analogues of these complexes have also been synthesized (the imine is reduced to a secondary amine or reductively aminated to give the tertiary amine) and are active for polymerization of lactide.[66] A half-salan based ligand developed by Hillmyer and Tolman was a landmark catalyst for the polymerization of LA; it was the most active catalyst at the time of the report.[65] The high activity of the tridentate system was attributed to facile coordination of LA to the less coordinatively saturated metal centre.

β-Diiminate complexes have also received a large amount of attention as catalysts for polymerization. Analogues of magnesium,[25, 89, 90] tin,[91] iron[63] and zinc[25, 89, 90, 92] catalysts have been reported. In general, these catalysts display the characteristics of living systems. The magnesium β-diiminate catalysts are among the most active catalyst currently known for the metal-mediated ring-opening polymerization of LA; the zinc systems are also highly active and exhibit some stereoselectivity in the polymerization. [65]

1.4 Stereoselectivity in polymerization

As mentioned earlier in the discussion of the biodegradability of PLA, the microstructure of a polymer can have a very significant impact on its macroscopic properties. There are a number of different microstructures that are possible for polymers. The stereoselectivity in olefin polymerizations has been extensively studied since Natta discovered that metal-based catalyst could control the stereoregularity of olefin polymerization.[93] To date a large number of systems are available for the controlled polymerizations of olefins. For olefin polymerization one variance in microstructure is based on regioisomerism, which is based on the number of head-to-head, head-to-tail and tail-to-tail linkages in the polymer backbone. Different microstructures can also be based on the stereochemical configuration of the polymer. If the given monomer for a polymerization is optically active (i.e. it is chiral) or pro-chiral the resulting polymer can be optically active. In this case the relative configuration of chiral centres in the polymer backbone determines the microstructure. A chain that contains sequential stereocentres of the same relative stereochemistry is isotactic while a chain that contains sequential alternating stereocentres is syndiotactic. If a chain exhibits no regularity in the relative stereocentres then the polymer is atactic.

NMR spectroscopy of polymers is a very powerful technique in the determination of polymer microstructure.[94] Short polymer sequences such as triads, tetrads, pentads, or hexads (a triad is a sequence of three monomer units, a tetrad is a sequence of four monomer units, etc) can be assigned to their various stereosequences based on their distinct chemical shifts. The stereosequences are labeled according to the type of linkages in the monomer sequences. A linkage between monomers can be either meso or racemic: a meso linkage indicates that the two monomers have the same relative stereochemistry; a racemic linkage indicates that the two

adjacent monomers have opposite stereochemistry (Figure 1.1). Both ^{1}H NMR and ^{13}C $\{^{1}H\}$ NMR have been used extensively to analyze polymers, and with the advances in two-dimensional techniques COSY, HETCOR, and NOESY have become increasingly used in the analysis of polymers. Nuclei such as ^{13}C, ^{31}P, and ^{15}N nuclei are particularly useful for assigning stereosequences; their wide chemical shift ranges allow for better resolution of peaks, and assignment of more complex microstructures.

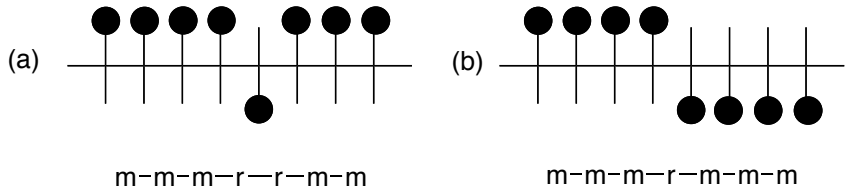

Figure 1.1 Schematic representations of two possible forms of propagation errors: (a) enantiomorphic site control error, (b) chain end control error.

Two mechanisms are possible for stereoselective polymerizations by single-site metal-based catalysis: enantiomorphic site control and chain-end control. In enantiomorphic site control a chiral catalyst will selectively polymerize one enantiomer of a monomer preferentially over the opposite enantiomer. In chain-end control the stereoselectivity of the polymerization is controlled by the chirality of the last incorporated monomer in the growing chain. The mechanism by which stereocontrol is achieved is hard to determine; the polymers resulting from the two mechanisms can have very similar microstructures. As well, the two mechanisms can act in tandem to provide the observed stereocontrol. This interaction between chain end control and site control can either be constructive (increasing the stereoselectivity) or destructive (decreasing the stereoselectivity).

Stereoerrors occur during polymerization for systems that are not ideal. Occasionally the "wrong" enantiomer is incorporated. The way these stereoerrors are propagated in the growing polymer chain can provide invaluable evidence for determining which mechanism is responsible for stereoselectivity. In the case of enantiomorphic site control once an error occurs it is corrected by the selectivity of the catalyst, and the "right" enantiomer continues to be polymerized, while in chain end control, the enantiomer being polymerized is switched once an error occurs (Figure 1). Errors introduced during chain-end control can lead to stereoblocks the length of which are determined by the degree of selectivity exhibited by the catalyst; the more selective the catalyst the larger the length of the isotactic blocks.

Mathematical models have been used in order to understand the way in which polymers propagate. From these models probabilities for the different stereosequences can be calculated. The two most common models are the Bernoulli trial and first-order Markov steps. By definition a Bernoullian system involves two possible events each with a given probability of occurring (Figure 1.2). In this case, the two events are either a meso or racemic linkage being formed with the probability for each of these events being P_m and P_r. These probabilities are independent of the previous event; the chirality of the next incorporated monomer is independent of the chain end. This corresponds to a system in which enantiomorphic site control is the method by which stereoselectivity is achieved. In contrast, for the Markov model the probability of the next event occurring is dependent on the current state of the system; therefore for a two-event system (the formation of either a meso or racemic linkage) there are four different probabilities $P_{m/m}$, $P_{m/r}$, $P_{r/r}$. and $P_{r/m}$. The Markov model is used to describe probabilities in a chain-end controlled polymerization. Higher order Markov models take into account the stereochemistry of additional chain units.

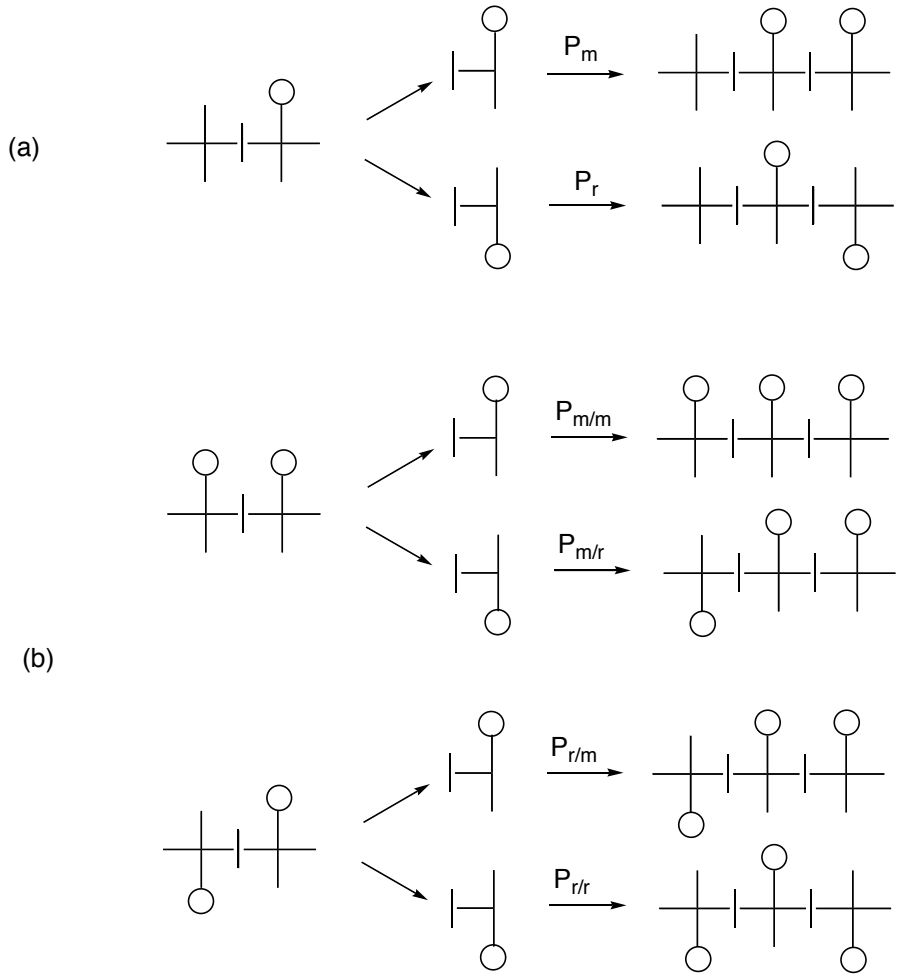

Figure 1.2. Schematic representation of propagation mechanisms (a) Bernoullian (b) first-order Markov

1.5 Stereoselectivity in the polymerization of LA

Lactide contains two stereocentres; therefore a large number of microstructures are possible in the ROP of lactide. In addition to isotactic, syndiotactic, and atactic polymers, microstructures containing heterotactic PLA, stereoblocks of PLA, as well as stereocomplexes of PLLA and PDLA can be formed (Chart 1.4).[70] It is possible to form isotactic, heterotactic, stereoblock, and stereocomplexes of PLA from the polymerization of *rac*-lactide. In the case of heterotactic PLA the monomer being polymerized must alternate after each ring-opening event. Syndiotactic PLA

can only be synthesized from meso-LA; the only way to obtain perfectly alternating stereocentres in the backbone is if the monomer itself contains both an R, and an S-centre. The catalyst then has to preferentially ring-open one stereocentre of the *meso*-lactide in order to obtain the syndiotactic polymer.[95] If the catalyst alternates which acyl bond is cleaved for *meso*-LA then a heterotactic microstructure is obtained.[92] Isotactic PLA can be obtained by polymerizing enantiopure monomer or by the chiral resolution of *rac*-LA using an enantioselective catalyst. It has been shown that *rac*-Salen catalysts can be used to polymerize rac-LA to produce stereocomplexes of PLLA and PDLA. In this case the R-catalyst polymerizes D-LA preferentially to form PDLA, and the S-catalyst polymerizes L-LA to form PLLA.[71-73, 82]

Chart 1.5. Possible microstructures of PLA

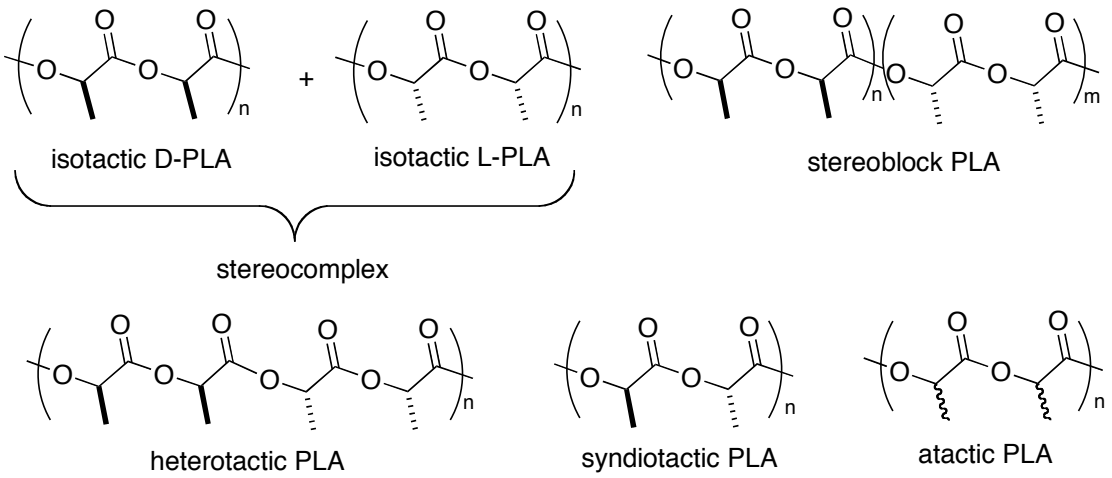

Three methods are possible for the formation of stereoblock PLA. Control of the feedstock by sequential addition of first D-LA followed by L-LA upon complete conversion of the D-LA can produce stereoblock isotactic PLA. The polymerization of *rac*-lactide with

enantiopure catalyst can also produce isotactic stereoblock PLA, although in this case the microstructure is most likely a tapered stereoblock with the percent composition of the two monomers changing over the length of the chain. Alternatively, a chain transfer mechanism has been proposed to explain the experimental observation of the formation of stereoblock PLA from the polymerization of *rac*-LA with *rac*-catalyst. Coates proposes that rapid chain transfer occurs between two enantiomers of the catalyst. He uses the relative ratio of different stereosequences in the polymer backbone to justify the proposed mechanism.[40]

The ^{1}H NMR spectrum of a sample of PLA contains two sets of peaks corresponding to the methine and methyl protons. The methine protons only couple to the adjacent methyl protons, and are observed as a number of overlapping quartets, while the methyl region is composed of overlapping doublets. Homonuclear decoupling experiments are commonly used for simplifying the ^{1}H NMR spectra of PLA samples. In these experiments the methyl region is constantly irradiated in pulses during the collection time. This constant irradiation saturates the excited state for the methyl protons, eliminating spin-spin coupling relaxation processes with the methine protons. Without the coupling to the methyl protons the overlapping quartets are simplified to a series of singlets in the methine region. These singlets correspond to different tetrad sequences: rrr, mmm, mrm, rmr, mmr, rmm, rrm, and mrr.

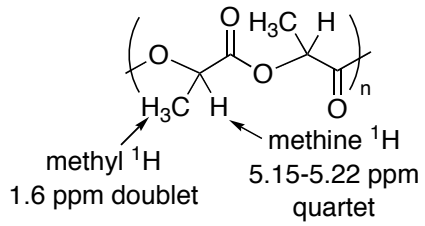

Figure 1.3. ^{1}H NMR characteristics of PLA.

Polymer samples that are obtained from the polymerization of *rac*-LA can contain five of these singlets: mmm, mrm, rmr, mmr, and rmm. It should be noted that two peaks are observed for the mmr, and the rmm tetrads but the two stereosequences are indistinguishable by ^{1}H NMR. The rrr, rrm, and mrr are only observed if *meso*-LA is polymerized or if scrambling of the stereocentres occurs during polymerization either by racemization of the monomer or by scrambling of the chains via transesterifcation. The homonuclear decoupled ^{1}H NMR of heterotactic PLA contains two peaks of the same relative intensity corresponding to the rmr and mrm stereosequences, while syndiotactic and isotactic PLA contain only one resonance corresponding to stereosequences of rrr and mmm respectively. The rmr, mmr, and rmm sequences are present in atactic PLA, or in isotactically enriched PLA that contains stereoerrors (Chart 1.5). Stereoerrors in syndiotactic or heterotactic PLA will give the rrm, mrr stereosequences. By examining the relative integration of the tetrads it is possible to determine both the overall microstructure of the polymer sample and the mechanism by which stereoselectivity is occurring.

Chart 1.6: Stereosequences of PLA: (a) syndiotactic PLA (b) heterotactic PLA (c) isotactic PLA (d) isotactic PLA with stereoerror (enantiomorphic site control) (e) isotactic PLA with stereoerror (chain end control)

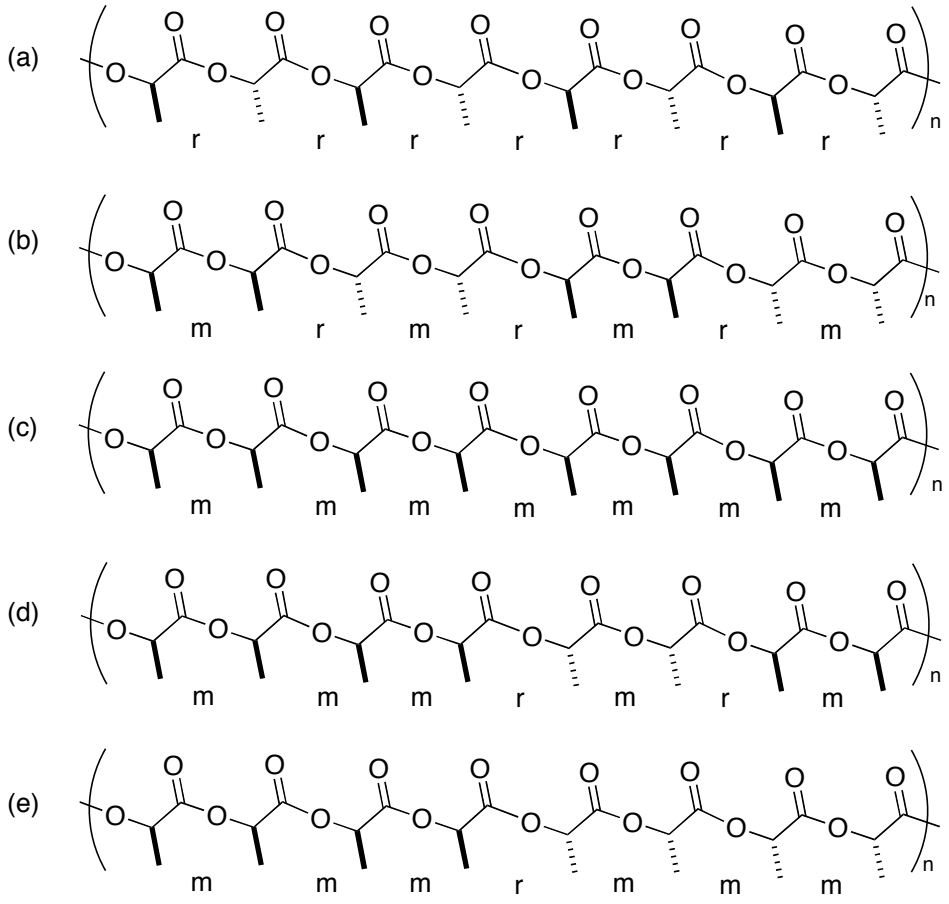

As was discussed previously, the way in which stereoerrors are propagated during polymerization can elucidate the mechanism behind the stereoselectivity of a given catalyst. In the case of PLA if the stereocontrol is due to enantiomorphic site control the ratio for the relative integration of the tetrads will be 1:2:1:1 for mmr, mrm, rmr, and rmm (Chart 5). When chain end control is the mechanism by which stereocontrol is achieved isotactic stereoblocks are formed and the rmr tetrad is absent while the remaining sequences are found in a ratio of 1:1:1 (mmr, mrm, rmm). [40, 94]

The relative integration of the different stereosequences in the polymer can also be used to determine the probability of a meso (P_m) or racemic (P_r) linkage forming during the polymerization (Table 1.1).[25, 94] These values can then be correlated to the overall microstructure: P_m values close to one indicate entirely isotactic PLA, and P_r values close to one indicate entirely syndiotactic PLA. Heterotactic PLA also has a P_r value of one since linkages formed during polymerization of *rac*-lactide, and not the inherent linkages in the monomer contribute to the value of P_r. The assignment of r and m linkages in the polymer backbone is shown in Chart 5, and is based on connections between lactic acid subunits in the polymer chain (not lactide units).

Table 1.1. Probability of tetrad sequences in PLA based on Bernoullian Statistics.

	Probability	
Tetrad	*rac*-LA	*meso*-LA
[mmm]	$P_m^2 + P_rP_m/2$	0
[mmr]	$P_rP_m/2$	0
[rmm]	$P_rP_m/2$	0
[rmr]	$P_r^2/2$	$(P_m^2 + P_rP_m)/2$
[rrr]	0	$P_r^2 + P_rP_m/2$
[rrm]	0	$P_rP_m/2$
[mrr]	0	$P_rP_m/2$
[mrm]	$(P_r^2 + P_rP_m)/2$	$P_m^2/2$

Analysis of the methine and carbonyl regions of the ^{13}C NMR spectrum has also been used to determine the microstructure of PLA samples; the carbon NMR is used to confirm the assignment from the homonuclear decoupled ^1H spectrum. In the ^{13}C NMR spectrum the hexad stereosequences are resolved in the carbonyl region, and the most commonly used assignments were made by Kasperczyk.[15] The resolution in the methine region is slightly lower although assignment at the tetrad level can be achieved. The P_r and P_m values can also be calculated from

the intensity of the ^{13}C NMR peaks analogous to the methods used for the homonuclear decoupled spectra.

A number of catalysts have been shown to be stereoselective in the polymerization of lactide. Several chiral catalysts have been shown to exhibit enantiomorphic site control in the polymerization of *rac*-LA to produce isotactic PLA. These include the chiral aluminum salen complexes used by Coates *et al*. In this case a binapthyl backbone was used to create a symmetric salen ligand, Feijen *et al* later used a diaminocyclohexane moiety in the salen ligand to produce another stereoselective catalyst.[67, 73] In contrast achiral salen,[69, 74] and salan complexes have been shown to be stereoselective in the polymerization of lactide via chain end control. Bulky β-diiminate zinc complexes[25, 29] and the sterically bulky calcium complexes of trispyrazolyl hydroborate[34] are also stereoselective via a chain-end control mechanism. Other complexes with bulky ligands such as the trisphenolate titanium[96] or the amine trisphenolate germanium complexes[75] have also demonstrated good stereoselctivity via chain end control. An interesting thiol containing salen type complex of scandium synthesized by Okuda and co-workers, shows chain-end stereocontrol of the polymerization through fluxionality in the ancillary ligand.[56] The catalysts that exhibit chain end control usually produce heterotactic PLA from the polymerization of *rac*-LA. [25, 29, 34, 42, 56, 92, 96]

Chart 1.7: Representative catalysts for (a) enantiomorphic site control and (b) chain end control in the stereoselective polymerization of lactide.

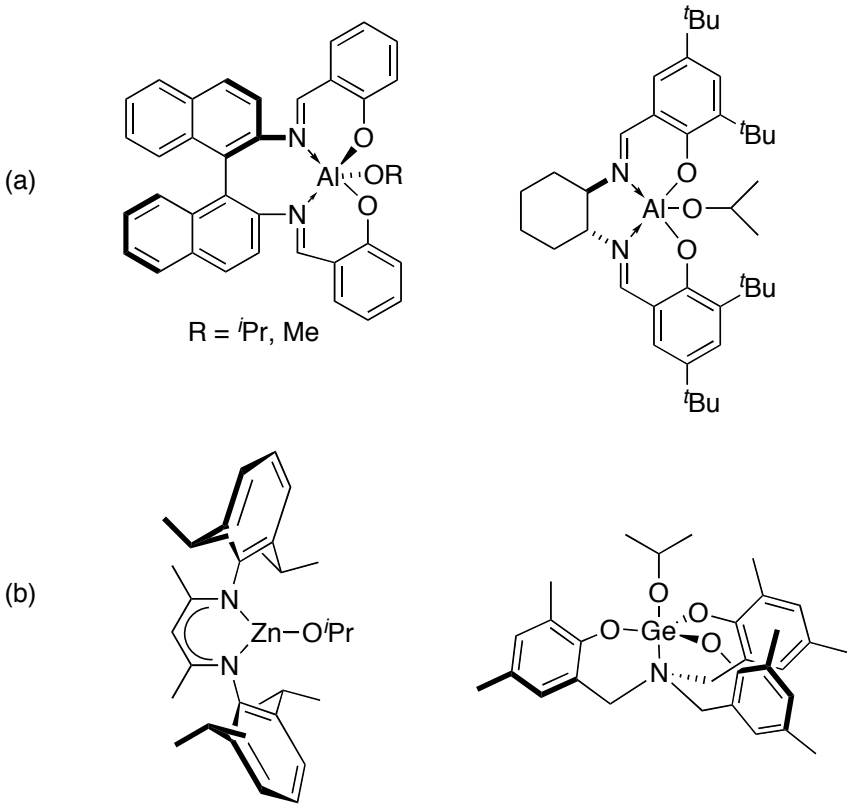

The previously discussed NHC organocatalysts also exhibit moderate stereoselectivity in the polymerization of LA.[23] The P_m values for the systems range from 0.55 to 0.59 for reactions carried out at 25 ºC depending on the steric bulk of the substituents on the nitrogens of the carbene, with the highest values being obtained for mesityl substitution. When the reaction is cooled down to -70 ºC this stereoselectivity increases up to 0.9 for the value of P_m indicating that almost entirely isotactic segments of PLA have been formed. A chiral carbene was used in order to see if enantiomorphic site control could play a role in the stereoselectivity of the polymerization but no greater control was observed; this supports a chain-end control mechanism for the stereoselectivity of all the catalysts including the chiral carbene.

1.6 General Chemistry of Indium and Group 13 Metals

The success of aluminum catalysts for the stereoselective and controlled ROP of LA has led us to investigate the activity of indium complexes in this role. However, group 13 elements are varied in their reactivity and properties.[97] Boron is perhaps the most obvious outlier when it comes to Group 13. It is a covalently bonded non-metallic insulator, while aluminum, gallium, indium and thallium are soft metals with low melting points, and low resistivity. The valence electronic configuration for the group is ns^2np^1. For Ga and In the valence orbitals also contain a filled d-orbital, and Tl possesses a filled f-orbital. Boron is also amphoteric in nature, while aluminum and gallium are only minimally amphoteric, and indium is even less so. The group displays an unusual trend in ionization energies (B > Tl > Ga > Al > In). For Groups 1 and 2 an increase in ionization energy is observed with an increase in atomic number; however, for Group 13 this trend is interrupted at both gallium and thallium due to d-block contraction and f-block contraction respectively. The electronegativiy of the atoms increases from Al to Tl.

For compounds of Group 13 elements the most common oxidation state is the +3 oxidation state. Thallium is the exception with its most common oxidation state being +1. This is attributed to a decrease in stability of the +3 oxidation state with increased atomic size; the energy required to involve the ns^2 electrons in bonding is greater than the energy released in the formation of the bonds. The relative stability of the +1 oxidation state for Group 13 metals increases down the group: Al < Ga < In < Tl. Tl tends to behave more like the alkali metals in its reactivity. It is highly basic and upon exposure to air it forms TlOH and hydrogen gas.

The Lewis acidity of the Group 13 metals follows the general trend: $AlX_3 > GaX_3 > InX_3$ (X = halogen) with $AlCl_3$ being the most Lewis acidic. Depending on the nature of the atom that is acting as an electron donor (N, O, or S) the acceptor ability of the metal changes. In terms

of polarizability B and Al are considered hard acceptors, and Ga and In are considered soft. For donation from nitrogen or oxygen containing compounds the above trend is observed, but when sulfur-containing donors are used the large more polarizable gallium becomes the strongest acceptor ($GaX_3 > AlX_3 > BX_3$ (X = Cl, Br)). For neutral adducts of the trihalides the stoichiometry for monodentate ligands is generally 1:1 for Al and Ga (MX_3L). However for In the most common stoichiometry is 1:3 (MX_3L_3).

Elemental indium is naturally occurring, but was not isolated in large amounts until the 20th century. It is the least abundant of the Group 13 elements; it is found in the earth's crust with an abundance of 0.05 ppm.[98] China and Canada are two of the top exporters of indium, which is isolated as a by-product in the smelt processing of zinc. Demand for indium has increased in recent years due to its extensive use in the materials industry. Indium tin oxide (ITO) films are used in light emitting diodes (LEDs) and accounted for 84% of the global consumption of indium. Low molecular weight indium complexes such as trimethylindium have been used in the semiconductor industry as precursors in metal vapor deposition of thin films. The price for elemental indium has risen from $170 US/kg in 2003 up to $918 US/kg in 2006.

The coordination chemistry of indium is not as well known as that of aluminum or even gallium. The natural abundance (8.3% by weight of the Earth's crust) and low cost of aluminum have played a role in the amount of research in aluminum chemistry.[97] This along with its notable success in many catalytic processes has led to extensive research into many of the aspects of aluminum chemistry. In contrast, the relatively expensive and less available indium has not received such interest; although, it has garnered notice recently as a robust and interesting Lewis acid for organic catalytic transformations.

From the late 1990's to early 2000's an exponential growth was seen in the number of

organic transformations carried out using InX_3 (X = Cl, Br, I, or OTf) as a Lewis acid catalyst. [99-102] Indium has been used in many different types of reactions including additions, cyclizations, aromatic electrophilic substitutions, rearrangements, and coupling reactions. The transformations can usually be carried out under mild conditions with high yields and in some cases very high selectivity. One of the most exciting aspects of this chemistry is the notable water tolerance of the indium salts.[100] This allows in some cases for the reaction to be carried out in water or for the catalyst to be recovered.

Very few discrete indium complexes have been used to carry out the aforementioned transformations. A chiral (S)-Binol indium catalyst has been used for the asymmetric allylation of carbonyl compounds. The chiral catalyst gives good enantioselectivity, and is tolerant of small amounts of water in the system (7.4 equivalents).[100] This promising start to indium complexes playing a role in enantioselective catalysis prompted us to propose a chiral indium complex for the polymerization of lactones as the goal for this work.

A recently published example by Huang and co-workers demonstrated that indium compounds could be active in the polymerization of caprolactone.[103] Ancillary ligands based on a substituted pyrrole ((2-dimethylaminomethyl)pyrrolate) were used to encapsulate the metal. The chosen initiator groups were methyl, chloride, and pyrrole ligands. Crystal structures were obtained for two of the complexes (the methyl and pyrrole derivative). These showed that both complexes had distorted trigonal bipyramidal geometry.

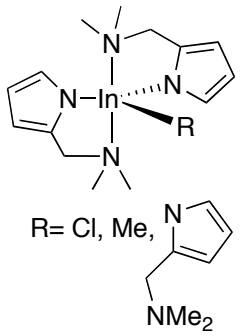

Figure 1.4. Indium catalysts for the polymerization of ε-caprolactone.

All three compounds successfully catalyzed the ring-opening polymerization of ε-caprolactone. To our knowledge this is the only example of an indium catalyst ring-opening polymerizing lactones, prior to the results presented in this thesis. ε-Caprolactone is perhaps the easiest of the lactones to polymerize; there is no steric bulk on the ring to slow coordination, and the ROP is more thermodynamically favorable. No mention is made of attempts to polymerize other monomers, and complexes with better initiator groups such as alkoxides were not synthesized.

The polymer samples were analyzed by GPC in order to determine their molecular weight and molecular weight distributions. The lowest molecular weight distribution was seen for the chloride-initiated polymerization at room temperature (1.45) while the largest distribution was observed for the pyrrole-initiated polymerization (1.99). These values could be improved upon lowering the temperature at which the polymerization occurred (0 ºC), and worsened by elevating the reaction temperature (60 ºC). The yield of polymer was high, but the molecular weights do not match expected values for metal mediated single site chain growth; the values are much lower than expected.

Goals of this Work

The goals of this work were to expand upon the known chemistry of indium by developing new chiral indium complexes, and to expand the scope of Group 13 complexes that act as catalysts for the polymerization of lactide. It was hoped that incorporation of indium in the catalyst would result in a highly active, functional group tolerant, robust catalyst. To this end a series of chiral tridentate indium complexes were synthesized, and their activity towards the polymerization of lactide was explored.[104]

CHAPTER 2. THE SYNTHESIS OF INDIUM COMPLEXES.

2.1 Introduction

As discussed in Chapter 1, a metal catalyst for the ROP of lactide the compound must have the general formula of L_nMR where L_n represents a non-labile ancillary ligand set, and R represents an initiator group. The ancillary ligand that we chose for our indium catalysts was 2-[[[(dimethylamino)cyclohexyl]amino]methyl]-4,6-bis(tert-butyl)phenol (H_2NNO), previously reported by Finney, et al.[105]

The tridentate ligand is a chiral version of the ligand used by Hillmyer and Tolman in their highly active achiral zinc catalyst.[65] It has been demonstrated that chiral aluminum catalysts have exhibited a marked stereoselectivity for the ROP of *rac*-lactide. However, these aluminum-based systems demonstrated low activity compared to the zinc systems.[67] Therefore we hoped to combine these characteristics and develop a highly active and stereoselective Group 13 catalyst by using a chiral tridentate pro-ligand.

Two different synthetic approaches for the formation of indium complexes are known. The first method is via protonolysis of either a trialkyl[106-109] or triamido-indium[110-112] compound via elimination of an alkane or an amine, respectively. The second route is via a salt metathesis reaction of the sodium, lithium, or potassium salts of the ligand and an indium trihalide.[103, 113-115] In this work both routes were attempted with varying degrees of success (Scheme 2.1). In order to generate a catalyst, we anticipated that an alkoxide would have to be introduced at a later stage via reaction with either an alcohol (protonolysis route) or a metal alkoxide (salt metathesis route).

Scheme 2.1. Proposed routes to the synthetic target.

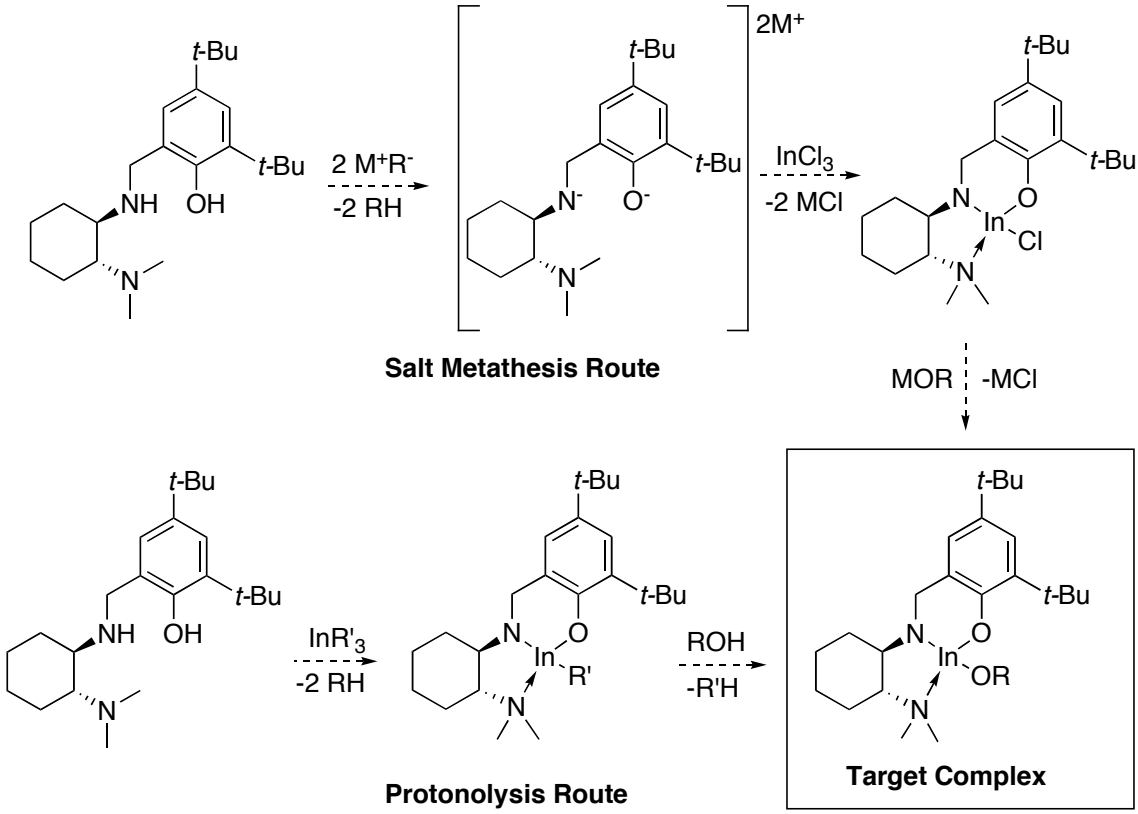

2.2 Results

The synthesis of H_2NNO was modified from the reported literature synthesis.[105] Purification steps were added at the imine and the amine stage in order to obtain a pure product, and the use of sodium cyanoborohydride was eliminated in the final step of the ligand synthesis. Instead the more cost effective reagent sodium borohydride was used for the reduction of the imine to a secondary amine (Scheme 2.2).

Scheme 2.2. Synthesis of 2-[[[(dimethylamino)cyclohexyl]amino]methyl]-4,6-bis(tert-butyl) phenol

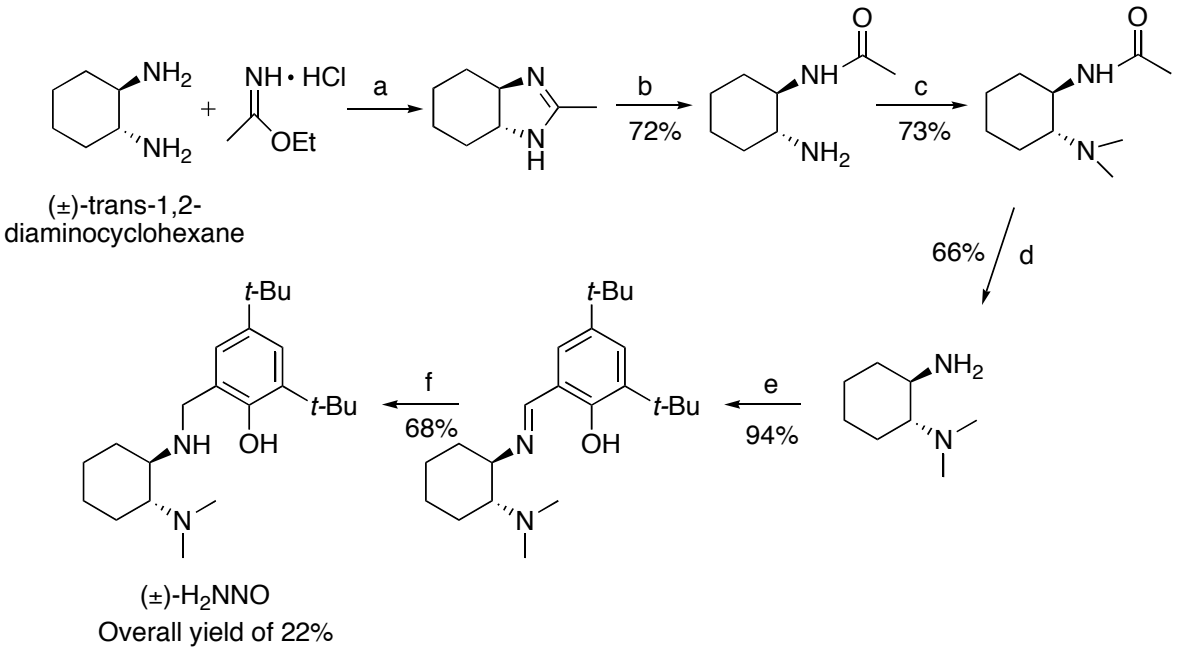

a. EtOH; b. EtOH/H_2O, D; c. formaldehyde, $NaBH_3CN$, AcOH, CH_3CN;
d. 4M HCl; e. 3,5-di-tert-butyl-2-hydroxybenzaldehyde, MeOH; f. $NaBH_4$, CH_3CN

Ligand synthesis involves the formation of an asymmetric diamine from (±)-1,2-trans-diaminocycloxhexane ((±)-DACH), via a protection/deprotection route. An imidazole ring is formed from the reaction of the (±)-DACH with the Pinner salt ethylacetimidate hydrochloride.

This product is hydrolyzed to give an asymmetric acylated product. The primary amine is methylated in a reductive amination using sodium cyanoborohydride and formaldehyde. The acyl protecting group is removed under acidic conditions to reform a primary amine, which is functionalized via a condensation reaction to form an imine. The final step in the synthesis is to reduce the imine to a secondary amine via reduction with sodium borohydride. The enantiopure analogue of the ligand RR-H_2NNO was also prepared. In this case RR-DACH was isolated from (±)-DACH by formation of the diastereomeric salt with L-tartaric acid, using the methodology developed by Jacobsen and co-workers.[116]

The first attempts to form this complex from the prepared pro-ligand, H_2NNO, followed a protonolysis route, adapted from literature.[114] Starting from indium trichloride, trimethyl indium was formed *in situ* from reaction with three equivalents of methyl lithium (Scheme 2.3). Addition of H_2NNO to this mixture formed a dimethylated species, (NNO)$InMe_2$ (**1**) as opposed to the expected monomethylated indium complex (for simplicity NNO^- is defined as the monodeprotonated ligand NN_HO^- where the secondary amine remains protonated). Complex **1** was isolated in a 40% yield as a white solid. The ^{1}H NMR and ^{13}C NMR spectra of **1** showed the expected signals for both the bound HNNO as well as the two methyl groups bound to indium, with characteristic upfield signals near 0 ppm. Crystals of **1** suitable for single crystal X-ray diffraction were grown from diethyl ether (-35 ºC); the ORTEP diagram is shown in Figure 2.1. The molecule shows a distorted square-based pyramidal geometry, with the tridentate ligand bound in a meridional fashion.

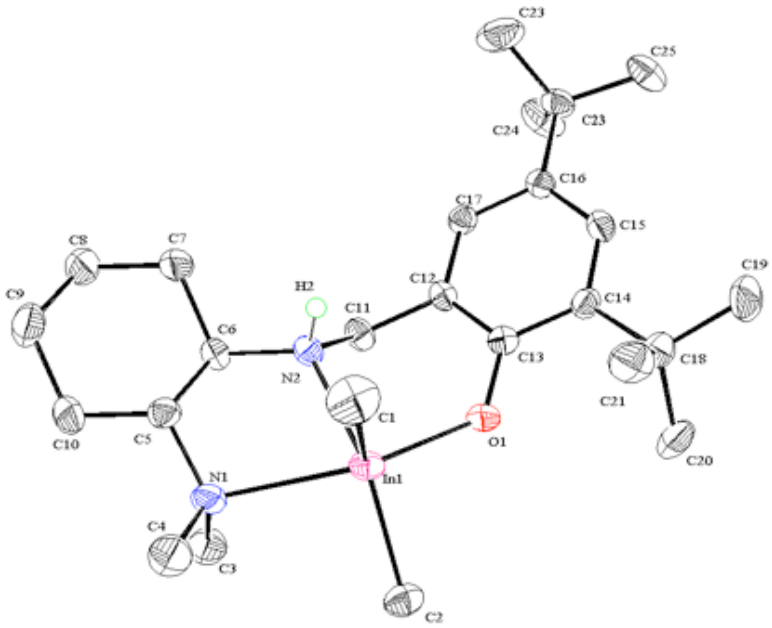

Figure 2.1. ORTEP view of (NNO)$InMe_2$ (**1**). Most hydrogen atoms are omitted for clarity and thermal ellipsoids are drawn at 50% probability.

Table 2.1. Selected interatomic distances (Å) for compound **1**.

Bond	Length (Å)
N1-In1	2.503(2)
N2-In1	2.3549(18)
C1-In1	2.161(2)
C2-In1	2.150(2)
O1-In1	2.1521(15)
C4-N1	1.469(3)
C5-N1	1.481(3)

Table 2.2. Selected bond angles (°) for compound **1**.

	Angle (°)		Angle (°)
C2-In1-O1	91.41(8)	C1-In1-N2	96.17(9)
C2-In1-C1	127.15(10)	C2-In1-N1	91.15(8)
O1-In1-C1	108.15(9)	O1-In1-N1	141.60(6)
C2-In1-N2	135.96(7)	C1-In1-N1	100.51(9)
O1-In1-N2	80.66(6)	N2-In1-N1	71.20(6)

Interestingly, the secondary amine does not deprotonate to form a monomethyl complex. This lack of reactivity could be due to the low acidity of the secondary amine, or steric constraints which do not allow the proton of the secondary amine and the $-CH_3$ to become close enough to eliminate methane. When complex **1** is heated in either coordinating (THF) or non-coordinating (toluene) solvents under static vacuum no further reaction is observed. Preliminary attempts were made to form an indium alkoxide complex from **1**. When the compound was reacted with either one or two equivalents of a secondary alcohol isopropanol no reaction was observed. Even when using a large excess of ethanol at room temperature for two hours no indium-alkoxide product was observed, and only starting material was recovered. These results confirm the lower polarity and greater covalent nature of the indium-carbon bond and show that the indium-bound methyl fragment cannot act as a strong enough base in the reaction to form the alkoxide.

In our attempts to synthesize **1** an interesting by-product was isolated. Early attempts to recrystallize **1** from pentane resulted in the formation of the compound (NNO)$InMe_2$•$InClMe_2$ (**2**). From X-ray analysis of a single crystal of the compound it was determined that a mixed species had been formed from the combination of **1** and partially reacted Me_2InCl. In the crystal structure it can be seen that dinuclear species had been formed from the combination of **1** and partially reacted Me_2InCl. The structure shows the ligand phenolic oxygen acting as a bridging ligand between the two indium atoms (Figure 2**)**. The second metal centre (In2) has a distorted tetrahedral geometry while the metal coordinated to the NNO ligand (In1) has a distorted square-based pyramidal geometry, as was seen in the crystal structure of **1**. The distance between In1 and Cl1 (3.774 Å) falls just outside the sum of the van der Waal radii for indium and chlorine

(3.75 Å) indicating that there may be some interaction or attractive forces between the two atoms.

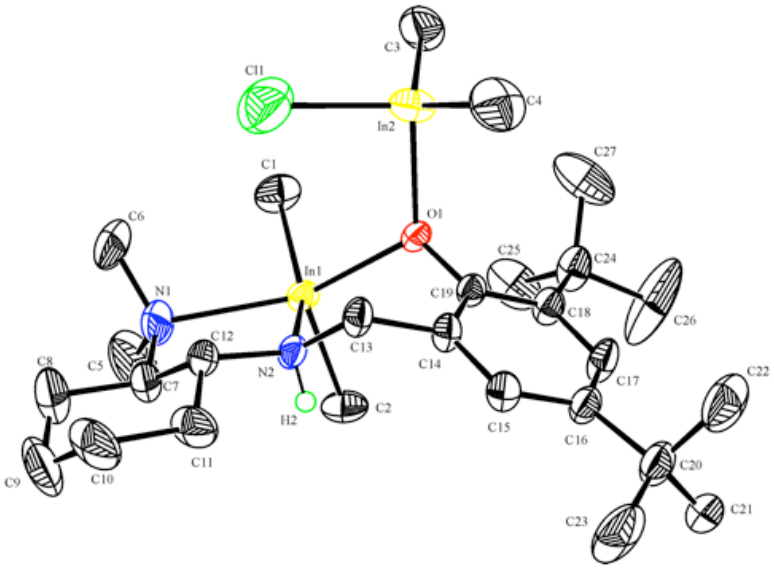

Figure 2.2. ORTEP view of (NNO)InMe$_2$•InCl(Me)$_2$ (**2**). Most hydrogen atoms and solvent molecules (pentane) are omitted for clarity and thermal ellipsoids are shown at 50% probability.

Table 2.3. Selected interatomic distances (Å) for compound **2.**

Bond	Length (Å)	Bond	Length (Å)
N1-In1	2.430(4)	C2-In1	2.127(5)
N2-In1	2.315(3)	C3-In2	2.110(5)
O1-In2	2.194(3)	C4-In2	2.104(5)
O1-In1	2.227(3)	C5-N1	1.460(7)
In2-Cl1	2.3668(18)	C6-N1	1.454(7)
C1-In1	2.120(4)		

Table 2.4. Selected bond angles (°) for compound **2**.

	Angle (°)		Angle (°)
In2-O1-In1	120.49(11)	O1-In1-N1	142.27(13)
C1-In1-C2	125.2(2)	N2-In1-N1	72.25(13)
C1-In1-O1	91.46(15)	C4-In2-C3	126.3(2)
C2-In1-O1	104.62(16)	C4-In2-O1	103.28(18)
C1-In1-N2	142.22(17)	C3-In2-O1	108.60(19)
C2-In1-N2	92.38(17)	C4-In2-Cl1	109.17(19)
O1-In1-N2	81.67(11)	C3-In2-Cl1	108.55(16)
C1-In1-N1	92.82(18)	O1-In2-Cl1	96.88(8)
C2-In1-N1	103.28(18)		

Alternative protonolysis routes were also attempted (Scheme 2.3). The trialkyl starting material tris(isobutyl) indium (III) was also synthesized from isobutylmagnesium bromide and indium trichloride. The bulky starting material was then reacted with H_2NNO. It was hoped that the steric crowding at the metal centre would provide the driving force for the second deprotonation of the ligand causing elimination of isobutane. Unfortunately, the reaction never produced a clean product, and resulted in an intractable mixture of products. This was perhaps due to impure starting material; Schlenk equilibria are known to occur during metal-Grignard reactions resulting in a mixture of mono-, di- and tri- alkylated salts of the metal. [117]

Scheme 2.3. Protonolysis routes to indium complexes

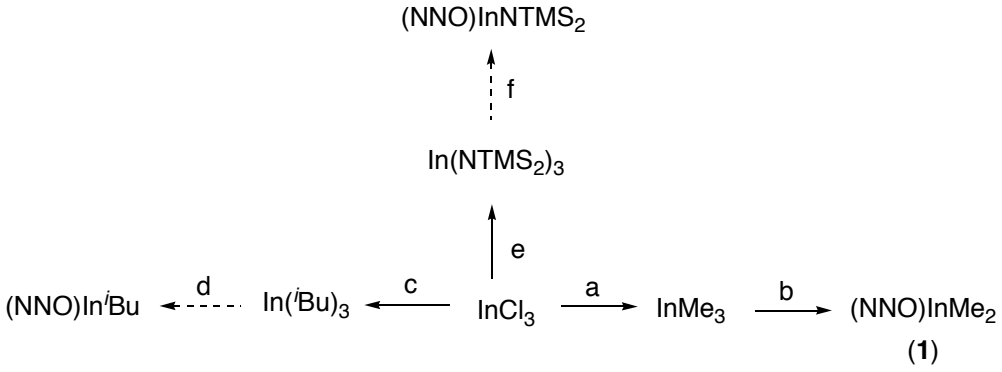

a. 3 MeLi, Et_2O; b. H_2NNO, Et_2O; c. ^{i}BuMgBr, Et_2O; d. H_2NNO;
e.$NaNTMS_2$, Et_2O; f. H_2NNO

Since both the alkyl starting materials did not follow the desired synthetic route indium starting material with potentially more basic substituents capable of deprotonating both the phenolic and secondary amine protons was synthesized. The starting material tris-

(bistrimethylsilylamido) indium (III) was synthesized from the sodium salt of the amide and indium trichloride using a published procedure.[118] The reaction of the indium triamide with H_2NNO resulted in a mixture of products under a variety of conditions, and a single product was never isolated from the mixture.

At this point, the alternative salt metathesis route for the synthesis of the target complex was attempted. The first step in this route, as shown in Scheme 1, is the deprotonation of the ligand to form a salt of the pro-ligand. The most common route used to deprotonate compounds for inorganic synthesis is through the use of *n*-butyllithium or hydrides of either sodium or potassium. A number of reagents were used as bases to deprotonate the pro-ligand including n-butyllithium, potassium hydride, and benzylpotassium. Despite a number of attempts to deprotonate the ligand only the monodeprotonated pro-ligand, HNNO, was isolated. This strongly suggests that the central nitrogen of the pro-ligand is simply not acidic enough to be deprotonated.

The related pK_a values for a number of organic compounds are shown in Table 2.5.[119] It can be seen that a secondary amines (*i*-Pr_2NH and TMS_2NH) have a pK_a of approximately 30-40, while toluene (the conjugate acid of benzylpotassium) has a pK_a of 41 or 43 depending upon which solvent is used to measure the value. From this data, one might assume that benzyl potassium could in fact deprotonate the secondary amine of the H_2NNO pro-ligand. Possibly the formation of the charged NNO^{2-} compound is disfavored because of the destabilizing effect of having two anions close together on the molecule. Alternatively, the weak acidity of the secondary amine could be attributed to a highly stable six membered ring being formed upon hydrogen bonding of the proton of the secondary amine to the phenolic oxygen. This "proton sponge effect" might increase the stability of the monodeprotonated state and cause a lower

acidity for the amine.

Table 2.5. pK_a values for simple organic compounds

		pK_a *		
Entry	Substrate	THF	H_2O	DMSO
1	MeOH		15.5	27.9
2	*t*-BuOH		17.0	29.4
3	NH_3		38	41
4	*i*-Pr_2NH	36		
5	TMS_2NH	26		30
6	Ph_2NH			25
7	$PhCH_3$		41	43
8	CH_4		48	56
9	$(Me)_2CH_2$		51	

*Values >14 for water and >35 for DMSO were extrapolated by various methods

In one attempt to deprotonate H_2NNO in diethyl ether using two equivalents of benzylpotassium. A mixture of the monopotassiated salt, KH(NNO), and potassium ethoxide was isolated. The potassium ethoxide was produced *in situ* from the deprotonation of diethyl ether. This pathway to the formation of alkoxides is known and is thought to occur via deprotonation of the β-carbon of the diethylether with elimination of ethylene.[120] When the mixture of potassium ethoxide and KH(NNO) was carried forward by reaction with indium trichloride a bridged dinuclear indium complex $[(NNO)InCl]_2(\mu\text{-OEt})(\mu\text{-Cl})$ (**3**) was formed (Scheme 2.4). The bridged complex shows the incorporation of one equivalent of ethoxide per two indium atoms (Scheme 4). This reproducible reaction was carried out in up to a 2 g scale and gave overall yields of 60-70% (based on the amount of $InCl_3$ used).

Scheme 2.4. Synthesis of compounds **3** and **4**.

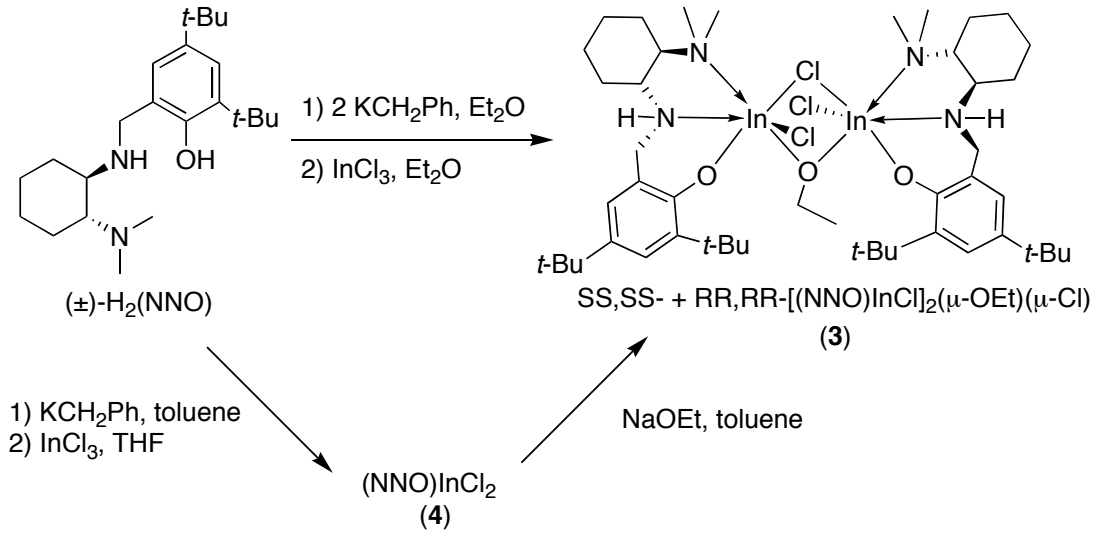

The solid state structure of **3** was obtained from single crystal X-ray diffraction (Figure 2.3). The structure shows chloride and ethoxide ligands bridging the two indium atoms. To our knowledge, this is the first example of this type of a mixed-bridge system for indium. Each indium centre has pseudo-octahedral geometry and a terminal chloride ligand. The ligand is acting as a monoanionic tridentate ligand and is bound in a facial fashion. Although the compound was formed from a racemic mixture of the pro-ligand, only homochiral complexes are formed. Although both homochiral enantiomers are observed in the lattice of the crystal only the structure of RR,RR-**3** is shown. The ^{1}H and ^{13}C NMR spectra show only one set of peaks for the ligand backbone, and ethoxide group, and provides no evidence for a mixed RR,SS-**3** being formed. When enantiopure H_2NNO is used to synthesize **3** identical NMR chemical shifts are observed.

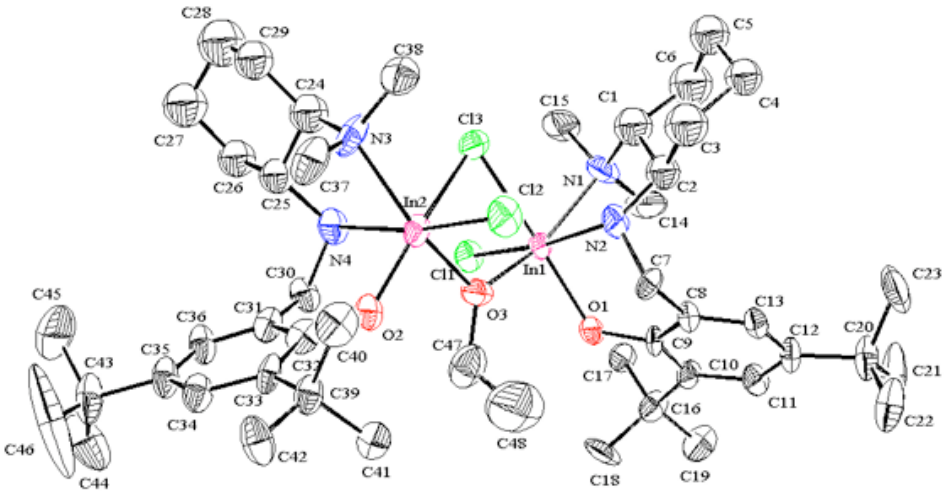

Figure 2.3. ORTEP view of $[(NNO)(Cl)In]_2(\mu\text{-}OEt)(\mu\text{-}Cl)$ (3). Hydrogen atoms omitted for clarity and thermal ellipsoids are shown at 35% probability.

Table 2.6. Selected interatomic distances (Å) for compound **3**.

Bond	Length (Å)	Bond	Length (Å)
N1-In1	2.334(10)	Cl1-In1	2.419(3)
N2-In1	2.257(8)	Cl2-In2	2.428(3)
N3-In2	2.354(10)	Cl3-In2	2.636(4)
N4-In2	2.269(9)	Cl3-In1	2.667(3)
O1-In1	2.084(7)	C14-N1	1.439(16)
O2-In2	2.050(8)	C15-N1	1.493(16)
O3-In1	2.112(8)	C37-N3	1.512(18)
O3-In2	2.129(8)	C38-N3	1.501(17)

Table 2.7. Selected bond angles (º) for compound **3**.

	Angle (º)		Angle (º)		Angle (º)
In1-O3-In2	118.1(3)	N1-In1-Cl1	94.0(3)	N4-In2-N3	77.9(4)
In2-Cl3-In1	86.62(9)	O1-In1-Cl3	166.8(2)	O2-In2-Cl2	94.7(2)
O1-In1-O3	93.0(3)	O3-In1-Cl3	77.1(2)	O3-In2-Cl2	94.8(2)
O1-In1-N2	88.2(3)	N2-In1-Cl3	83.5(3)	N4-In2-Cl2	170.4(3)
O3-In1-N2	91.8(3)	N1-In1-Cl3	86.2(3)	N3-In2-Cl2	92.7(3)
O1-In1-N1	102.1(3)	Cl1-In1-Cl3	92.89(10)	O2-In2-Cl3	168.1(2)
O3-In1-N1	161.4(3)	O2-In2-O3	93.0(3)	O3-In2-Cl3	77.6(2)
N2-In1-N1	78.0(4)	O2-In2-N4	89.0(3)	N4-In2-Cl3	84.5(3)
O1-In1-Cl1	96.7(2)	O3-In2-N4	93.8(4)	N3-In2-Cl3	85.5(3)
O3-In1-Cl1	94.9(2)	O2-In2-N3	102.8(4)	Cl2-In2-Cl3	93.30(12)
N2-In1-Cl1	171.4(3)	O3-In2-N3	161.8(4)		

A rational synthetic route to **3** was explored (Scheme 2.4). In this route the KHNNO was formed via direct reaction of the H_2NNO with one equivalent of benzylpotassium in toluene and reacted with indium trichloride to form (NNO)$InCl_2$ (**4**). When the reaction is carried out in a weakly or non-coordinating solvent (i.e. diethyl ether or toluene) multiple isomers of the product are seen by ^1H NMR spectroscopy. However, one isomer of the product is formed if THF or pyridine is used as the solvent for the reaction. In the spectrum of the pyridine adduct of **4** (**4**•Py) the relative integration of the aromatic protons of the pyridine molecule to the diastereotopic methylene protons of the backbone (-NH-CH_2-Ar) indicate a ratio of two pyridine molecules to one molecule of **4.** Upon crystallization of **4**•Py from a toluene/dichlormethane solution, the ratio is reduced to 1:1 and a single-crystal X-ray structure was obtained (Figure 2.4). The indium atom is in a pseudo-octahedral geometry, with the tridentate ligand bound in a facial fashion. The two chloride ligands are in a cis-geometry. Reaction of **4** with one equivalent of sodium ethoxide results in the formation of **3** in a 67% overall yield based on H_2NNO.

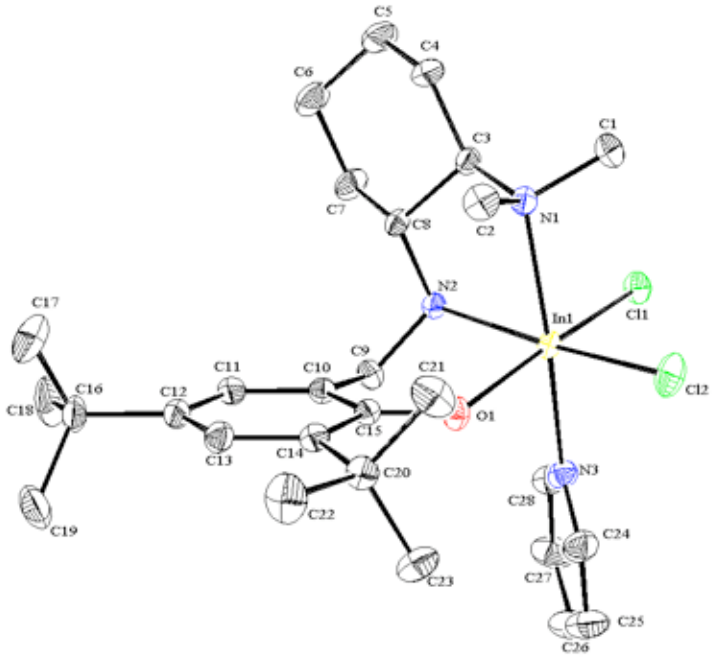

Figure 2.4. ORTEP view of (NNO)(Cl_2)In•Py (**4**•Py). Hydrogen atoms are omitted for clarity and thermal ellipsoids are shown at 50% probability.

Table 2.8. Selected interatomic distances (Å) for compound **4**•Py.

Bond	Length (Å)	Bond	Length (Å)
N1-In1	2.3415(12)	Cl1-In1	2.5164(4)
N2-In1	2.2663(12)	Cl2-In1	2.4025(4)
N3-In1	2.3136(13)	C1-N1	1.4855(19)
O1-In1	2.1187(10)	C2-N1	1.4827(18)

Table 2.9. Selected bond angles (°) for compound **4**•Py.

	Angle (°)		Angle (°)
O1-In1-N2	84.80(4)	N3-In1-Cl2	93.58(3)
O1-In1-N3	84.12(4)	N1-In1-Cl2	94.50(3)
N2-In1-N3	94.63(4)	O1-In1-Cl1	167.66(3)
O1-In1-N1	98.75(4)	N2-In1-Cl1	88.22(3)
N2-In1-N1	77.60(4)	N3-In1-Cl1	86.32(3)
N3-In1-N1	171.37(4)	N1-In1-Cl1	89.65(3)
O1-In1-Cl2	91.13(3)	Cl2-In1-Cl1	97.250(14)
N2-In1-Cl2	170.41(3)		

A solution of the dinuclear complex **3** is stable at room temperature under inert atmosphere in a variety of solvents. The compound appears to dissociate into a number of isomers upon reaction with coordinating compounds such as pyridine or methyl-(S)-lactate (an acyclic analogue of lactide). However, upon exposure to water the complex rapidly transforms to a bis-hydroxy complex $[(NNO)InCl(\mu\text{-}OH)]_2$ (Scheme 2.5). A single crystal suitable for X-ray diffraction was obtained by crystallization of **5** from acetonitrile (Figure 2.5).

Scheme 2.5**.** Synthesis of $[(NNO)InCl(\mu\text{-}OH)]_2$

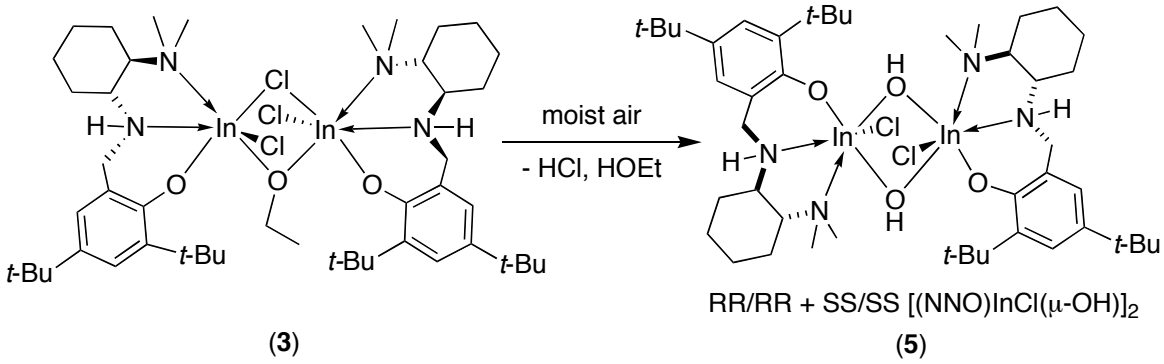

(**3**) (**5**)

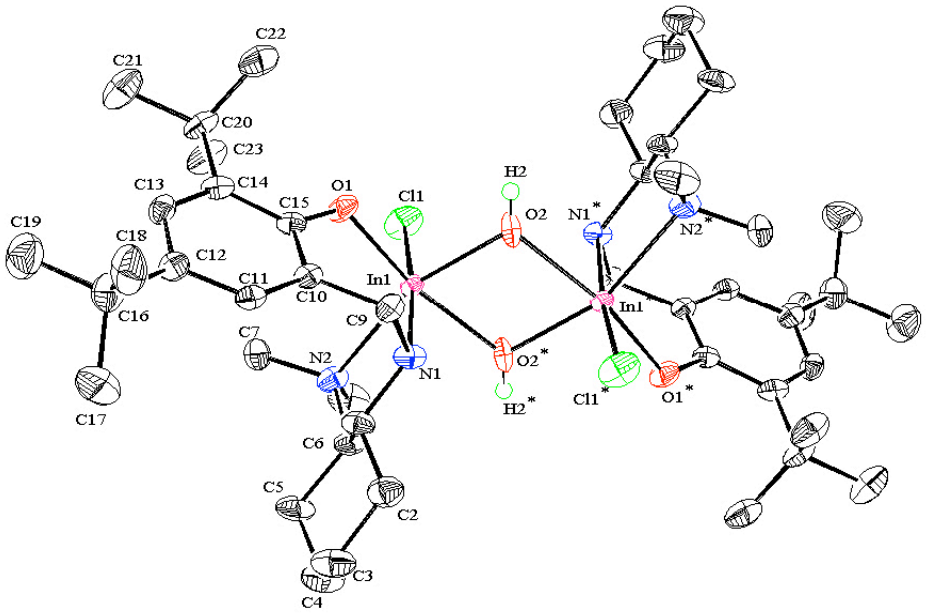

Figure 2.5. ORTEP view of $[(NNO)(Cl)In(\mu\text{-}OH)]_2$ (**5**). Most hydrogen atoms omitted for clarity, and thermal ellipsoids shown at 50% probability.

Table 2.10. Selected interatomic distances (Å) for compound **5**.

Bond	Length (Å)	Bond	Length (Å)
N1-In1	2.202(5)	Cl1-In1	2.4387(15)
N2-In1	2.333(4)	In1-O2*	2.215(4)
O1-In1	2.099(3)	C7-N2	1.451(7)
O2-In1	2.160(4)	C8-N2	1.485(7)
O2-In1*	2.215(4)		

Table 2.11. Selected bond angles (°) for compound **5**.

	Angle (°)		Angle (°)
In1-O2-In1*	104.67(19)	O2-In1-N2	159.77(15)
O1-In1-O2	90.96(15)	N1-In1-N2	76.78(15)
O1-In1-N1	88.15(16)	O2*-In1-N2	88.14(15)
O2-In1-N1	90.20(15)	O1-In1-Cl1	93.54(11)
O1-In1-O2*	164.92(15)	O2-In1-Cl	96.82(12)
O2-In1-O2*	75.33(19)	N1-In1-Cl1	172.74(12)
N1-In1-O2*	85.67(17)	O2*-In1-Cl1	94.32(11)
O1-In1-N2	103.83(15)	N2-In1-Cl1	95.96(12)

The solid state structure of **5** shows a dinuclear indium complex doubly bridged by hydroxy ligands. The two ligands are bound on opposing faces of the molecule, allowing for a

centre of inversion. The ligands are facially bound to the indium atoms in a pseudo-octahedral geometry. Both this bridging motif and the reaction of dichloride indium complexes with water to form bridged hydroxy complexes have been reported previously in literature.[115] Complex **5** can be synthesized reproducibly in a quantitative yield.

A similar reaction of **4** with adventitious water, resulted in the isolation of crystals of $[(NNO)(Cl)In]_2(\mu\text{-}OH)(\mu\text{-}Cl)$ (**6**) (Scheme 2.6). When a sealed NMR tube containing a sample of **4** in deuterated benzene was left on the bench-top over a month a slow air leak led to the crystallization of **6** (Figure 6). In the complex the two metal centres are bound by facially coordinated ligands in a pseudo-octahedral geometry. The structure is very similar to that seen for **3**. It is possible that this type of structure could be an intermediate in the conversion of **3** to **5**. However, no attempts were made to develop a rational synthesis for **6**.

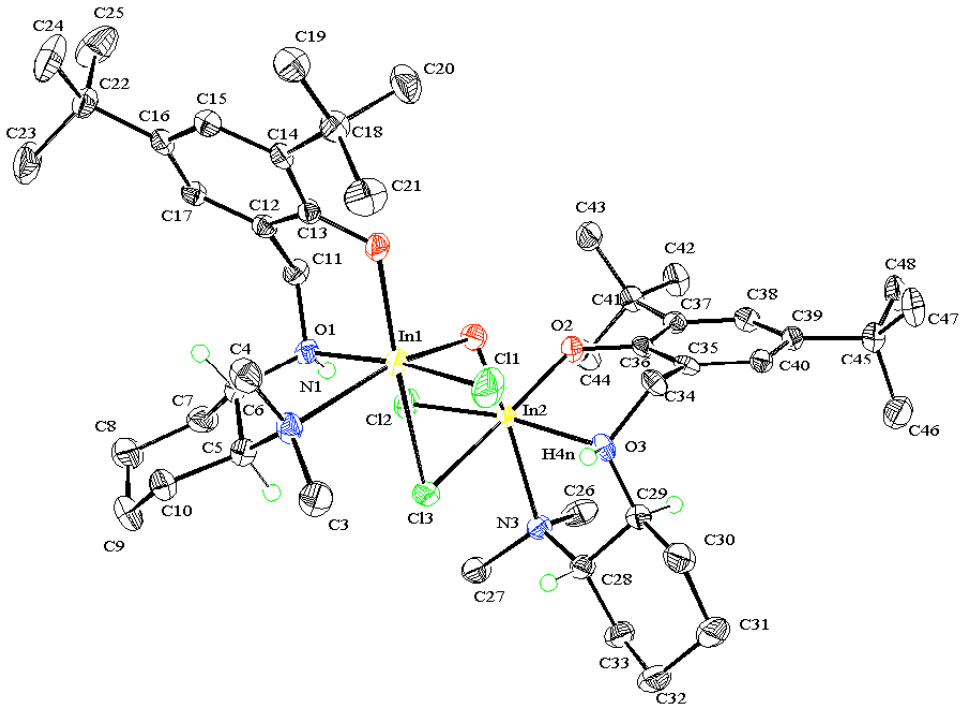

Figure 2.6. ORTEP view of $[(NNO)(Cl)In]_2(\mu\text{-}OH)(\mu\text{-}Cl)$ (**6**). Hydrogen atoms are omitted for clarity and thermal ellipsoids are shown at 50% probability.

Table 2.12. Selected interatomic distances (Å) for compound **6**.

Bond	Length (Å)	Bond	Length (Å)
N1-In1	2.359(3)	Cl1-In1	2.4084(9)
N2-In1	2.255(3)	Cl2-In2	2.4226(9)
N3-In2	2.324(2)	Cl3-In2	2.6657(8)
N4-In2	2.260(3)	Cl3-In1	2.6902(8)
O1-In1	2.086(2)	C3-N1	1.487(4)
O2-In2	2.074(2)	C4-N1	1.478(4)
O3-In2	2.113(2)	C26-N3	1.477(4)
O3-In1	2.125(2)	C27-N3	1.486(4)

Table 2.13. Selected bond angles (º) for compound **6**.

	Angle (º)		Angle (º)		Angle (º)
In2-O3-In1	120.84(9)	N1-In1-Cl1	96.76(7)	N4-In2-N3	76.81(9)
In2-Cl3-In1	86.97(2)	O1-In1-Cl3	167.90(6)	O2-In2-Cl2	95.87(6)
O1-In1-O3	93.80(8)	O3-In1-Cl3	75.54(6)	O3-In2-Cl2	96.89(6)
O1-In1-N2	88.35(9)	N2-In1-Cl3	85.53(7)	N4-In2-Cl2	171.51(7)
O3-In1-N2	87.46(9)	N1-In1-Cl3	84.23(7)	N3-In2-Cl2	94.97(7)
O1-In1-N1	104.41(9)	Cl1-In1-Cl3	91.45(3)	O2-In2-Cl3	167.92(6)
O3-In1-N1	154.84(9)	O2-In2-O3	93.90(8)	O3-In2-Cl3	76.26(6)
N2-In1-N1	76.04(9)	O2-In2-N4	88.16(9)	N4-In2-Cl3	84.96(7)
O1-In1-Cl1	95.84(6)	O3-In2-N4	90.28(9)	N3-In2-Cl3	85.13(7)
O3-In1-Cl1	98.53(6)	O2-In2-N3	102.96(9)	Cl2-In2-Cl3	92.30(3)
N2-In1-Cl1	172.42(7)	O3-In2-N3	158.25(9)		

Scheme 2.6. Proposed route to the formation of $[(NNO)(Cl)In]_2(\mu\text{-}OH)(\mu\text{-}Cl)$ (**6**)

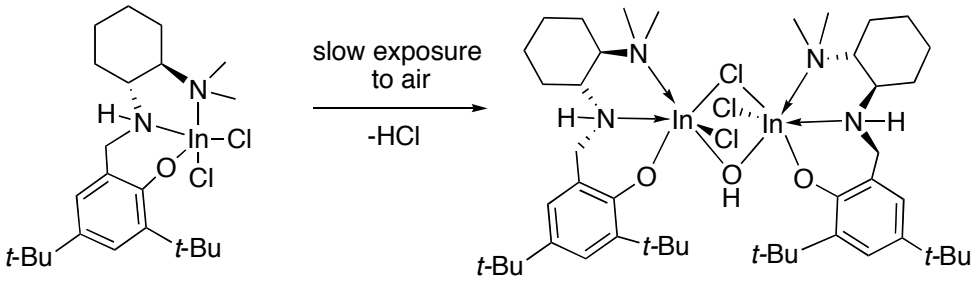

RR- + SS-(**4**)

RR/RR + SS/SS
$[(NNO)(Cl)In]_2(\mu\text{-}OH)(\mu\text{-}Cl)$
(**6**)

Attempts were made to synthesize a mononuclear indium alkoxide complex from complexes **4** and **3** (Scheme 2.7). To this end the dichloride indium complex **4** was reacted with both one and two equivalents of sodium ethoxide. As stated previously (Scheme 2.4) the reaction with one equivalent of sodium ethoxide gives the dinuclear complex **3** in high yields. Interestingly, the reaction of **4** with two equivalents of sodium ethoxide yields **3** as the major product. Other attempts with more basic alkoxides (potassium tert-butoxide or sodium tert-butoxide) led to multiple products. Attempts directly install a second alkoxide group on to **3** using potassium tert-butoxide as a base led to isolation of the starting material as the major component, which suggests that **3** is more thermodynamically favorable and stable than either the mononuclear (NNO)InCl(OEt) or the dinuclear $[(NNO)InCl(\mu\text{-}OEt)]_2$ complex which contain one ethoxide per indium atom.

2.3 Conclusion

A number of new indium complexes were synthesized and isolated. The complexes all contained a tridentate N,N,O-based ligand. The ligand is chiral containing (±)1,2-trans-DACH moiety in the backbone. It is the first time to our knowledge that this compound, 2-[[[(dimethylamino)cyclohexyl]amino]methyl]-4,6-bis(tert-butyl)phenol, has been used as a ligand. Crystal structures were obtained for four isolated products as well as two impurities. The majority of these structures show octahedral geometry at the metal centre (the exception being the dimethylated indium complexes **2** and **3**). The complexes also tend to form dinuclear structures with either oxygen based bridging ligand (hydroxy-, or alkoxy ligands) or chloride bridging ligand. This is a common motif in other indium chemistry. Complex **3** was shown to convert cleanly to complex **5** in the presence of water.

The ligand did not bind as expected to the metal centres. It was hoped that the tridentate ligand would be dianionic in nature, with both the phenolic proton and the proton of the secondary amine being acidic enough to be removed either prior to attachment to the metal (salt metathesis route) or upon attachment to the metal (protonolysis). In all the cases observed here the ligand was monoanionic. The phenolic proton was deprotonated via both routes, but the proton of the secondary amine could not be removed via either route.

A dinuclear indium ethoxide complex **3**, $[(NNO)(Cl)In]_2(\mu\text{-}OEt)(\mu\text{-}Cl)$, was obtained via the direct reaction of a mixture of salts, KH(NNO) and KOEt, with indium trichloride. The synthetic methodology was further explored and it was found that the complex could also be obtained by direct reaction of $(NNO)InCl_2$ and NaOEt. In fact this complex seems to be unusually thermodynamically stable and is the major product in numerous attempts to synthesize a mononuclear indium complex.

2.4 Experimental

General Considerations.

Unless otherwise indicated, all air- and/or water-sensitive reactions were carried out under dry nitrogen using either an MBraun glovebox or standard Schlenk line techniques. NMR spectra were recorded on a Bruker Avance 400MHz spectrometer. ^{1}H NMR chemical shifts are given in ppm versus residual protons in deuterated solvents as follows: δ 7.27 $CDCl_3$, δ 7.16 C_6D_6. $^{13}C\{^{1}H\}$ NMR chemical shifts are given in ppm versus residual ^{13}C in solvents as follows: δ 77.2 $CDCl_3$, δ 128.4 C_6D_6

Materials.

Solvents (pentane, THF, toluene, dichloromethane, and diethyl ether) were degassed and dried using 3Å molecular sieves in an mBraun Solvent Purification System. The THF was further dried over sodium and distilled under N_2. CD_2Cl_2 and $CDCl_3$ were dried over CaH_2, and degassed through a series of freeze-pump-thaw cycles. C_6D_6 was dried over sodium and degassed using a series of freeze-pump-thaw cycles. $InCl_3$ was purchased from Strem Chemicals and used without further purification. For the enantiopure catalyst the (±)-trans-1,2-diaminocyclohexane was resolved using Jacobsen's method,[116] and then carried forward through the same procedures as used for the *rac*-catalyst. The benzyl potassium was synthesized using a modified literature procedure using *n*-butyl lithium (Aldrich), potassium *tert*-butoxide (Alfa Aesar) and toluene.[121] All other compounds were obtained from Aldrich and used without further purification.

The literature preparation of H_2NNO was modified as follows: two purification steps were added: the imine was recrystallized from warm acetonitrile, and the ligand itself was recrystallized from acetonitrile when it was formed.

Synthesis of (NNO)$InMe_2$ (**1**)

A 125 mL round bottom flask was charged with $InCl_3$ (0.100 g; 0.45 mmol) in 15 mL of Et_2O. 1.6M MeLi in Et_2O (0.85 mL, 0.45 mmol) was added dropwise to the stirring mixture, which was stirred at room temperature for a further 20 minutes. H_2NNO (0.163 g; 0.45 mmol) was then added to the mixture as a solution in Et_2O (15 mL). The reaction was heated at 30 ºC for 24 h, cooled to room temperature and filtered through celite. Concentration of the filtrate to ca. 15 mL resulted in the formation of a white precipitate that was isolated by filtration and washed with pentane (3 x 2 mL) and dried under high vacuum to yield **1** (92 mg; 0.18 mmol; 41% yield). ^{1}H NMR (400 MHz, $CDCl_3$): δ 7.22 (1H, d, J=3 Hz, Ar*H*), 6.82 (1H, d, J=3 Hz , Ar*H*), 4.31 (1H, t, J=10 Hz, R_2N-C*H*-CH_2), 3.59 (1H, d, J=7 Hz, NH-CH_2-Ar) 2.61(1H, d, J=12 Hz, NH-CH_2-Ar), 2.47(1H, m, -CH_2- of DACH), 2.21, (6H, br s, N-(CH_3)$_2$), 1.90 (3H, m, -CH_2- of DACH), 1.61 (1H, t, J=10 Hz, -CH_2- of DACH), 1.43 (9H, s, *t*-Bu), 1.28 (9H, s, *t*-Bu), 1.24 (1H, m, -CH_2- of DACH), -0.15 (3H, s, In-CH_3), -0.35 (3H, s, In-CH_3). ^{13}C{^{1}H} NMR (75 MHz, $CDCl_3$): δ163.9, 138.3, 133.0, 124.3, 123.7, 122.8, 66.8, 58.1, 53.8, 35.4, 33.9, 32.6, 32.0, 29.7, 25.2, 24.8, 21.5, -7.0, -7.2. EI-LRMS (m/z) calc'd for $C_{25}H_{45}InN_2O$ [M^+] 504.26; found: 504.

Synthesis of [(NNO)InCl]$_2$(μ-OEt)(μ-Cl) (**3**)**.**

A 500 mL round bottom flask was charged with H_2NNO (1.000 g; 2.775 mmol) in 100 mL of Et_2O and cooled to -34 ºC. Benzyl potassium (0.722 g; 5.55 mmol) in 25 mL Et_2O was cooled to -34 ºC and added drop-wise to the stirring solution. The reaction was warmed to room temperature and stirred for a further 48 h. An off-white solid was isolated by filtration using a cintered frit, and dried under high vacuum for approximately 2 h. A 500 mL round bottom flask was charged with $InCl_3$ (0.608 g; 2.75 mmol) in 125 mL Et_2O to this stirring mixture was added the solid from the previous reaction as a slurry in 25 mL of Et_2O. The mixture was stirred at

room temperature for 48 h, and filtered through celite. The filtrate was concentrated to dryness, and the resulting residue was taken up in pentane resulting in a white precipitate which was isolated by vacuum filtration, and dried under high vacuum for 2 h to yield **3** (0.99g; 0.90mmol; 65%yield based on $InCl_3$ as the limiting reagent). ^{1}H NMR (400MHz, C_6D_6): δ 7.61 (1H, d, J=2.3Hz, Ar*H*), 6.8 (1H, d, J=2.2Hz, Ar*H*), 5.26 (1H, d, J=13.6Hz, NH-CH_2-Ar), 4.69 (1h, m, -OCH_2CH$_3$), 3.59 (1H, d, J=13.6Hz, NH-CH_2-Ar), 2.84 (1H, d, J=11.0Hz, R_2N-C*H*-CH$_2$-), 2.66 (1H, m, R_2N-C*H*-CH$_2$), 2.52 (3H, s, -N-CH_3), 2.42 (1H, br m, -CH_2- of DACH), 2.20 (1H, d, J=4.3Hz, -CH_2- of DACH), 1.95(2H, br m, -CH_2- of DACH), 1.83 (9H, s, -*t*Bu), 1.78 (3H, s, -N-CH_3), 1.56 (1H, t, J=6.7Hz, -O-CH$_2$-CH_3) 1.40 (9H, s, -*t*Bu) 1.20 (2H, br m, -CH_2- of DACH), 1.06 (1H, d, J=11.5Hz, -CH_2- of DACH) 0.61 (2H, br m, -CH_2- of DACH) 0.16 (1H, br m, -CH_2- of DACH). ^{13}C{^{1}H} NMR (75 MHz, C_6D_6): δ 163.9, 140.3, 137.4, 127.1, 125.4, 120.0, 65.6, 64.1, 53.3, 51.9, 51.2, 44.8, 39.0, 36.7, 34.9, 32.9, 31.5, 31.4, 25.4, 25.3, 22.2, 20.6. Anal. Calc'd (found) for $C_{48}H_{83}Cl_3In_2N_4O_3$: C 52.40 (51.96), H 7.60 (7.53), N 5.09 (5.03) %. X-ray quality crystals were grown from cold toluene over 1 week.

Synthesis of (NNO)$InCl_2$ (**4**).

A 250 mL round bottom flask was charged with a magnetic stir bar and a solution of H_2NNO (1.000 g, 2.78 mmol) in 20 mL cold toluene (-34 ºC). KCH_2Ph (0.361 g, 2.78 mmol) in 20 mL cold toluene was added dropwise as a slurry to the stirred solution. The reaction was warmed to room temperature and stirred for 16 h. The mixture was concentrated to dryness and the residue was taken up in 10 mL of pentane. A white solid precipitated from pentane and was isolated by filtration then dried under high vacuum for 2h to yield KHNNO (0.908 g, 2.28 mmol, 82% yield). 250 mL round bottom flask was charged with a slurry of $InCl_3$ in 30 mL cold THF (-34 ºC). KHNNO was added dropwise as a solution in 20 mL cold THF (-34 ºC) to the stirring $InCl_3$

mixture. The reaction was warmed to room temperature and stirred for 16 h then filtered through celite. The filtrate was concentrated to dryness taken up in 10 mL pentane. A white solid that precipitated out of solution was isolated by filtration and dried under high vacuum for 2 h to yield **4** (1.24g, 2.27mmol, 99% yield, 81% yield over two steps). ^{1}H NMR (400MHz, C_6D_6): δ 7.58 (1H, d, J=2.1Hz, Ar*H*), 6.75 (1H, d, J=1.9Hz, Ar*H*), 5.26 (1H, d, J=13.0Hz, NH-CH_2-Ar), 3.48 (1H, d, J=12.7Hz, NH-CH_2-Ar), 2.58 (1H, t, J=12Hz, -R_2N-C*H*-CH_2- of DACH), 2.40 (3H, s, -N-CH_3), 1.71 (9H, s, -*t*Bu), 1.67 (3H, s, -NCH_3), 1.35 (9H, s, -*t*Bu), 1.21 (1H, d, J=10.6Hz, -CH_2- of DACH), 1.12 (1H, d, J=11.5Hz, -CH_2- of DACH) 1.00 (1H, d, J=12.2Hz, -CH_2- of DACH), 0.61 (3H, m, -CH_2- of DACH), 0.11 (1H, q, J=12.1Hz, -CH_2- of DACH). ^{13}C{1H} NMR (75 MHz, C_6D_6): δ 163.92, 140.05, 137.85, 126.83, 125.43, 120.35, 65.71, 54.11, 51.72, 44.81, 38.67, 36.68, 32.89, 31.33, 31.05, 25.23, 24.94, 22.13. Anal. Calc'd (found) for $C_{23}H_{39}Cl_2InN_2O$: C 50.66 (50.43), H 7.21 (7.17), N 5.14 (5.04) %. EI-LRMS (m/z) calc'd for $C_{25}H_{39}Cl_2InN_2O$ [M^+] 544.15; found: 544. The pyridine adduct was formed by dissolving **4** in pyridine, with subsequent removal of the volatile solvent. X-ray quality crystals of **4**•Py were isolated by recrystallization from a toluene/dichloromethane mixture at room temperature.

Alternative synthesis of **3** from **4.**

A 125 mL round bottom flask was charged with NaOEt (37.5mg; 0.551mmol) in 20 mL toluene. A solution of **4** (0.300g, 0.551mmol) in 15mL toluene was added dropwise to this stirred mixture. The mixture was stirred at room temperature for 16 h, filtered through celite, and concentrated to dryness. The residue was taken up in 10 mL pentane from which a white solid precipitated. The solid was isolated by filtration to yield **1** (0.2551g, 0.23mmol, 83% yield, 67% over three steps). ^{1}H NMR (400MHz, C_6D_6): δ 7.61 (1H, d, J=2.3Hz, Ar*H*), 6.8 (1H, d,

J=2.2Hz, Ar*H*), 5.25 (1H, d, J=13.8Hz, NH-CH_2-Ar), 4.70 (1h, m, -OCH_2CH$_3$), 3.59 (1H, d, J=13.6Hz, NH-CH_2-Ar), 2.83 (1H, d, 11.0Hz, R_2N-C*H*-CH$_2$-), 2.66 (1H, m, R_2N-C*H*-CH$_2$), 2.51 (3H, s, -N-CH_3), 2.42 (1H, br m, -CH_2- of DACH), 2.20 (1H, d, 4.3Hz, -CH_2- of DACH), 1.95(2H, br m, -CH_2- of DACH), 1.83 (9H, s, -*t*Bu), 1.78 (3H, s, -N-CH_3), 1.60 (1H, t, 6.6Hz, -O-CH$_2$-CH_3) 1.39 (9H, s, -*t*Bu) 1.22 (2H, br m, -CH_2- of DACH), 1.06 (1H, d, J=11.5Hz, -CH_2- of DACH) 0.61 (2H, br m, -CH_2- of DACH) 0.16 (1H, br m, -CH_2- of DACH). ^{13}C{^{1}H} NMR (100MHz, C_6D_6): δ 163.9, 140.3, 137.4, 127.1, 125.4, 120.0, 65.6, 64.1, 53.3, 51.9, 44.8, 39.0, 36.7, 35.2, 34.9, 32.9, 31.5, 31.4, 25.4, 25.3, 22.2, 20.6.

Synthesis of [(NNO)InCl(μ-OH)]$_2$ (**5**)

Compound **1** was removed from an inert atmosphere and exposed to moist air for 48 h to yield the air and moisture stable compound **2** in quantitative yield. ^{1}H NMR (400mHz, C_6D_6): δ 7.71 (1H, d, J= 2.2Hz, Ar*H*), 6.85 (1H, d, J=2.2Hz, Ar*H*), 4.83 (1H, d, J=13.3H, -N-CH_2-Ar), 3.52 (1H, d, J=12.7Hz, -N-CH_2-Ar) 3.04 (1H, d, J=10.6Hz, -N-C*H*-CH$_2$-), 2.82 (1H, t, -N-C*H*-CH$_2$-), 2.59 (3H, s, -N-CH_3), 2.43 (1H, m, -CH_2- of DACH), 2.02 (2H, br m, -CH_2- of DACH) 1.97 (9H, s, -^{t}Bu), 1.81 (3H, s, -N-CH_3), 1.52 (9H, s, -^{t}Bu), 1.28 (2H, br m, -CH_2- of DACH), 1.13 (1H, d, J=12.7Hz, -CH_2- of DACH), 0.72 (3H, br m, -CH_2- of DACH) 0.23 (1H, m, -CH_2- of DACH). ^{13}C{^{1}H} (C_6D_6,100MHz): δ 163.8, 139.8, 137.5, 127.3, 125.3, 121.2, 65.7, 53.2, 51.9, 51.1, 44.9, 38.7, 36.7, 34.9, 32.9, 31.5, 31.4, 31.3, 25.3, 25.3, 22.1. ESI-LRMS (m/z) calc'd for $C_{46}H_{80}Cl_2In_2N_4O_4$ [MK$^+$] 1091.33; found: 1091.7. X-ray quality crystals were grown from acetonitrile at room temperature over the period of 1 week.

CHAPTER 3. KINETIC INVESTIGATIONS/POLYMER CHARACTERIZATION

3.1 Introduction

Monitoring reactions as they occur can provide useful data about how and why the reaction proceeds. In most cases, monitoring a reaction involves observing the formation of the product or the disappearance of the reagents. A simple reaction of a reagent, A, being converted to product, B, is shown below.

$$A \longrightarrow B$$

$$\text{rate} = -\frac{d[A]}{dt}$$

$$\text{rate} = \frac{d[B]}{dt}$$

In this case the rate of the reaction could be observed in two ways: one could observe the increase in concentration of B or the decrease in the concentration of A. Assuming that the reaction is first order with respect to A, it follows:

$$\text{rate} = k[A]$$

If we combine the two equations:

$$\text{rate} = k[A] = -\frac{d[A]}{dt}$$

$$\frac{d[A]}{[A]} = -kdt$$

$$[A] = [A]_0 e^{-kt}$$

where $[A]_o$ is the concentration of A at time zero. If the assumption holds that the rate is first

order with respect to the concentration of A, then a plot of the natural logarithm of [A] versus time should be linear with the following equation.

$$\ln([A] - [A]_0) = -kt$$

According to the Eyring equation the relationship between the natural logarithm of the observed rate (k) and the inverse of the temperature at which the reaction is carried out should be linear. The enthalpy ($\Delta H^{\ddagger}$) and the entropy of ($\Delta S^{\ddagger}$) activation are calculated from the slope of the line and the y-intercept respectively.[122]

$$\ln\left(\frac{k}{T}\right) = \frac{-\Delta H^{\ddagger}}{RT} + \ln\frac{k_b}{h} + \frac{\Delta S^{\ddagger}}{R}$$

where R = universal gas constant
k_b = Boltzmann's constant
h = Planck's constant

Combining these values and observations can lead to useful insights about the mechanism of the reaction. In order to obtain data, one must choose the appropriate spectroscopic technique to monitor the reaction.

The time-scale for the reaction often determines which technique will be used to monitor the process. If the process is on a femtosecond time scale then you cannot observe it using a technique that allows for collection of data every millisecond. Fortunately for polymer chemists the observable reaction time for most polymerizations is on the order of minutes, hours, or days. This means that a number of techniques are useful including UV, IR, and NMR spectroscopy. Observation of the ^{1}H nuclei by NMR spectroscopy remains one of the most useful techniques.

For the polymerization of lactide kinetic experiments are usually carried out using ^{1}H

NMR spectroscopy. The relative integration of the methine proton of the monomer is monitored over the course of the reaction. In CD_2Cl_2 at 298 K the methine proton of LA is a quartet located at 5.07 ppm, while the methine protons of the polymer fall in a range from 5.12 - 5.22 ppm. This chemical shift difference is large enough to resolve the monomer peaks from the peaks for PLA. As the polymerization proceeds a series of ^1H NMR spectra are obtained at regular time intervals. By measuring the integration of the LA methine proton as it is converted to PLA the rate for the overall reaction can be determined.

In order to obtain quantitative data from the NMR spectra an internal standard must be added to the reaction mixture. Several characteristics are important for an internal standard. It must not interfere with either the method of data collection, or the chemical processes that are occurring. For the polymerization of lactide 1,3,5-trimethoxybenzene (TMB) was chosen as the internal standard. It is reasonable to assume that TMB will not interfere with the polymerization, as it is unlikely to act as an initiator for the polymerization or as a chain transfer agent during polymerization. TMB is a relatively weak ligand and should not compete for coordination sites on the metal when in the presence of stronger ligands (ie. the ancillary ligand, or LA).

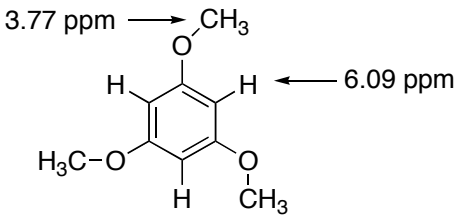

Figure 3.1. Internal standard (1,3,5-trimethoxybenzene) for the polymerization of LA and its ^1H NMR characteristics (CD_2Cl_2, 298K, 400MHz)

The chemical shifts for the internal standard must not overlap or interfere with any of the peaks that are being observed. TMB has only two peaks in the ^{1}H NMR spectrum (Figure 1). The first peak is a singlet at 3.77 ppm for the methyl protons. The second peak is also a singlet at 6.09 ppm corresponding to the aromatic protons. The two signals neatly bracket the region of interest for PLA but do not interfere with any of the peaks for the polymer. The peak for the methyl protons was used for calibrating the integration. Since the methyl peaks in TMB constitute 9 equivalent protons, a very small amount of the internal standard can be used relative to LA (molar ratio of 1:16 for TMB to LA).

In addition to the need for an internal standard, the temperature at which the polymerizations are performed must be known exactly in order to obtain high quality data for the construction of an Eyring plot. To this end, the temperature settings for the NMR probe must be calibrated at each temperature. The temperatures are calibrated using the values for the difference between the chemical shifts ($\Delta\delta$) of the two peaks in a given standard sample (provided by Bruker) and the equations given in Table 3.1.[123] Two standards are used for the desired temperature range; methanol is used for the lower temperature calibrations (230 – 300 K) and ethylene glycol is used for the higher temperature calibration (300-400 K).

Table 3.1. Equations for calibrating temperatures on NMR spectrometer

Standard	Temperature Range	Formula
4% MeOH in MeOH-d_4	230-270K	T(K) = -125.0($\Delta\delta$) + 490.0
	270-300K	T(K) = -114.83($\Delta\delta$) + 471.85
80% Ethylene Glycol in DMSO-d_6	300-400K	T(K) = -108.33($\Delta\delta$) +460.41

Analysis of the polymer samples is carried out using gel permeation chromatography (GPC). GPC is a form of size exclusion chromatography (SEC) a separation technique that separates compounds based on their size or molecular weight. The chromatography column is

packed with small particles of silica or polymers. These particles contain pores into which solute and solvent molecules can diffuse. Molecules that are larger than the average pore size are excluded and pass through the column quickly, while molecules that are smaller than the pore size are taken up in the pores and retained for longer periods on the column. Molecules of an intermediate size enter some but not all of the pores depending on their size. In this way molecules of different molecular weight are separated as they pass through the column. Multiple pieces of data can be determined by GPC analysis of polymers related to the samples molecular weight. These include the number average molecular weight (M_n), the weight average molecular weight (M_w), and the polydispersity index (PDI) or molecular weight distribution (MWD). PDI is defined as M_w/M_n.[124]

A calibration curve is normally used for determining the molecular weight of PLA samples. A series of polystyrene samples of known molecular weights are run on the instrument to construct a calibration curve. The samples of PLA are then analyzed and assigned a molecular weight based on where their retention time falls on the curve. This does not provide an absolute value for molecular weight (detection by laser light scattering provides absolute molecular weights), instead it is an approximation of the molecular weight. Laser light scattering detection for analysis of PLA is not generally used because of PLA's poor ability to scatter light (PLA has a low differential refractive index or d_n/d_c) and because the methodology has not been investigated as fully for polyesters as it has for other large molecules such as proteins.

All of the methods and techniques mentioned above were used, along with ^{1}H, ^{1}H{^{1}H}, and ^{13}C{^{1}H} NMR characterization of PLA samples, in order to describe the ROP of LA by complex **3**. The rate of polymerization was monitored by ^{1}H NMR spectroscopy and the molecular weight and polydispersity of the polymers were determined by GPC. The NMR

spectra of the polymers were used to assign the microstructure of the PLA samples and the mechanism by which the catalyst was exerting stereocontrol over the polymerization.[104]

3.2 Results

The dinuclear complex **3** is an active catalyst for the ring-opening polymerization of lactide. In polymerizations monitored to 90% conversion by ^{1}H NMR spectroscopy (25 ºC, CD_2Cl_2), 200 equivalents of *rac*-LA are converted to PLA in 30 min. This result is comparable to some of the most active metal-based catalysts reported to date and is significantly faster than aluminum salen complexes, which usually require several hours at elevated temperatures to convert LA under otherwise similar conditions.

It was previously shown that the dinuclear complex **3** dissociates in the presence of coordinating compounds. Therefore, we propose that at high concentrations of LA the dinuclear complex will split into two mononuclear fragments (NNO)$InCl_2$•LA (**4**•LA) and (NNO)InCl(OEt)•LA (**7**•LA). A control experiment shows that the mononuclear complex **4** is not a catalyst for the polymerization of lactide. Therefore, the mononuclear fragment **7**•LA is proposed as the active catalyst when the pre-catalyst **3** is used for the ring-opening polymerization of lactide (Scheme 3.1).

Scheme 3.1. Dissociation of **3** to generate the active catalyst **7**•LA.

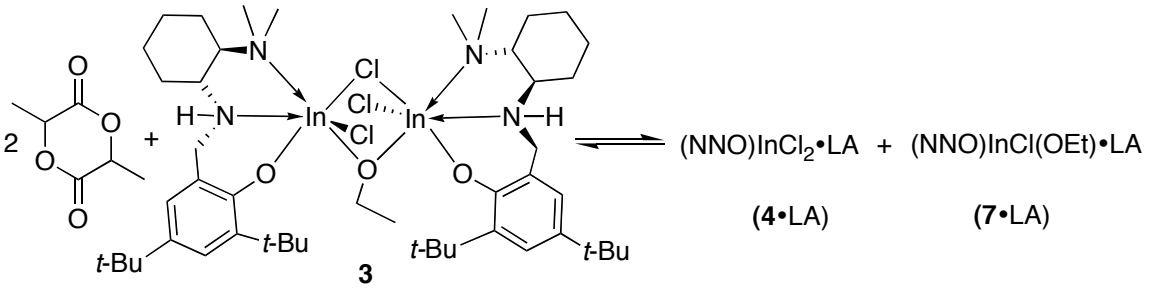

Complex **3** is also active for other lactone monomers including ε-caprolactone, and β-butyrolactone (Scheme 3.2). The polymerizations were performed in THF and complete conversion was achieved in less than 24 hours ([M]/[**3**] = 500). Preliminary GPC data on samples of the polymers show that the polymers have a narrow molecular weight distribution, and a close correlation is seen between the monomer loading and the molecular weight (Table 3.2). After attempts to establish the substrate scope, the work was directed towards elucidating the reactivity of **3** as a catalyst for LA polymerization. Kinetic studies were performed in order to determine the reaction order of the polymerization with respect to both the monomer and the catalyst and to determine the activation parameters ($\Delta H^{\ddagger}$ and $\Delta S^{\ddagger}$).

Scheme 3.2. Monomer scope for the polymerization of lactones by **3**.

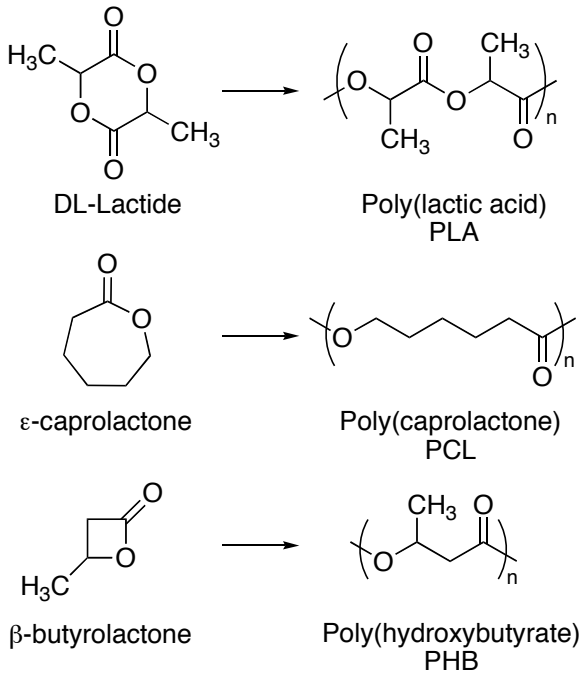

Table 3.2. GPC data for the polymerization of ε-caprolactone and β-butyrolactone by **3**.

Entry	Monomer (M)	[M]/[**3**]	M_n (calc'd)	M_n(expt)	M_W/M_N
1	ε-caprolactone	500	57000	61000	1.22
2	β-butyrolactone	500	43000	76000	1.41

GPC analysis of isolated polymer samples shows a linear relationship between added monomer ([LA]/[**3**]) and the observed molecular weight (M_n) (Figure 3.2). M_n closely follows the calculated molecular weight (illustrated by the straight line). The values for M_n(calc'd) were calculated assuming a single chain growing per molecule of **3** with complete conversion of monomer to polymer. This is in agreement with **7**•LA being the active catalyst for polymerization.

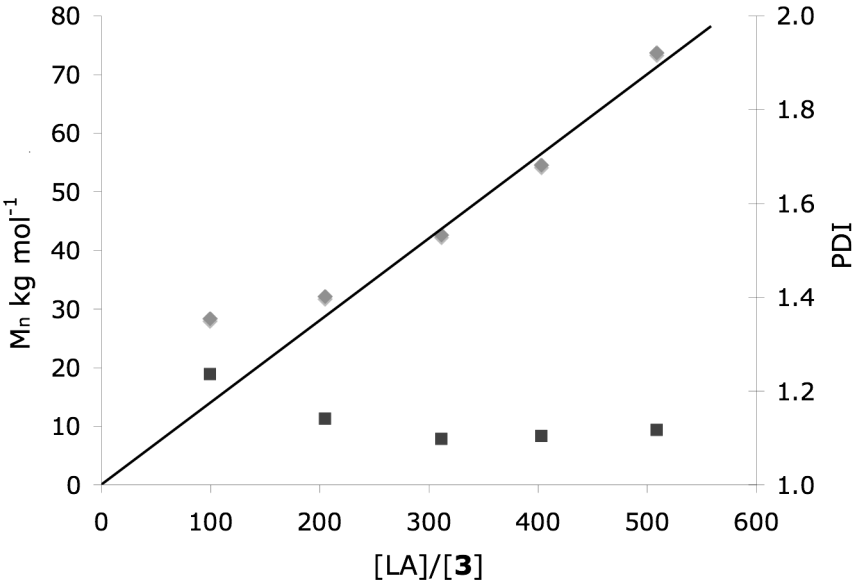

Figure 3.2. Plot of the observed molecular weight (M_n = ◆) and molecular weight distributions (PDI = ■) of PLA as a function of added monomer (calculated values for the molecular weights are shown using the line).

The PDI values obtained for the polymer samples are quite low (from 1.09-1.14) indicating that the system is well behaved. The small PDI values make it unlikely that transesterification processes, which result in larger values for PDI, are playing a significant role in the polymerization. The data for the polymer molecular weights and molecular weight distributions are indicative of a living system. However, two deviations in the data should be noted for the low monomer loading (100 equivalents): a relatively high value for the PDI (1.23) and a deviation between the calculated and observed M_n values (M_n(obs) = 28 000 g mol^{-1}; M_n(calc'd) = 14 000 g mol^{-1}).

A high M_n value suggests that fewer active sites are catalyzing the polymerization, while the high PDI value indicates that the number of active sites is not constant during polymerization. This apparent change in catalyst concentration could be attributed to an equilibrium between an active mononuclear catalyst and a dormant dinuclear species, similar to the one represented in Scheme 3.1. This would cause a decrease in the number of growing catalyst chains and a subsequent increase in the molecular weight and PDI.

Examination of the reaction *in situ* provides further evidence for the proposed mechanism. It was seen for the sequential addition of two aliquots of LA (100 equivalents each), that when the natural logarithm of the relative integration of the methine proton of LA is plotted versus time an initial curved region is observed indicating an induction period (Figure 3.3). This induction period is attributed to the equilibrium between **3** and the mononuclear species **4**•LA and **7**•LA. After the induction period, the plot becomes linear and first-order behavior is observed until approximately 90% conversion is achieved. Above 90% conversion, the slope decays exponentially until the reaction is complete. Upon addition of the second aliquot of monomer, no induction period is observed.

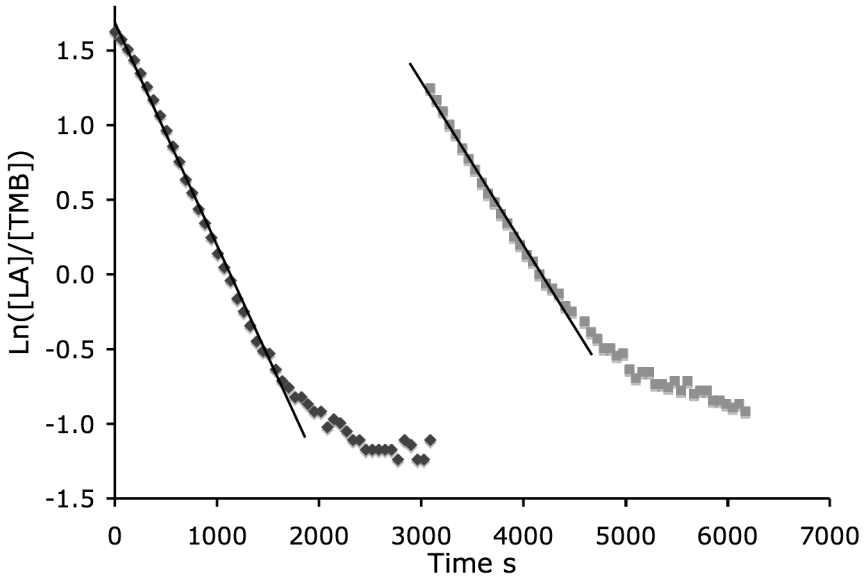

Figure 3.3. Plot of Ln([LA]/[TMB]) versus time for two sequential additions of LA (◆ = 1st addition of 100 equivalents; ■ = 2nd addition of 100 equivalents) (CD_2Cl_2, 298K, 400MHz)

The rate of polymerization was obtained from the slope of the line for the linear region of the graph. The rates of polymerization before (k = 0.56(0.18) s^{-1} M^{-1}) and after the second addition of monomer (k = 0.59(0.18) $s^{-1}M^{-1}$) were the same within error. The fact that the rate remains constant is a strong indication that the number of active catalyst sites did not decrease upon complete conversion to polymer. This information, along with the low PDI values and the linear relationship between molecular weight and catalyst loading, indicates that the catalyst system is living under the reaction conditions.

The rate of polymerization of LA is first order with respect to [**3**] (Figure 3.4). The rate also displayed first-order behavior towards LA one can therefore propose an overall second-order rate law.

$$\text{rate} = k\,[LA]\,[3]$$

This simplified rate law is an adequate description of the system for the bulk of the polymerization; however, it does not take into account the observed induction period for the catalyst or the decay in rate observed above 90% conversion.

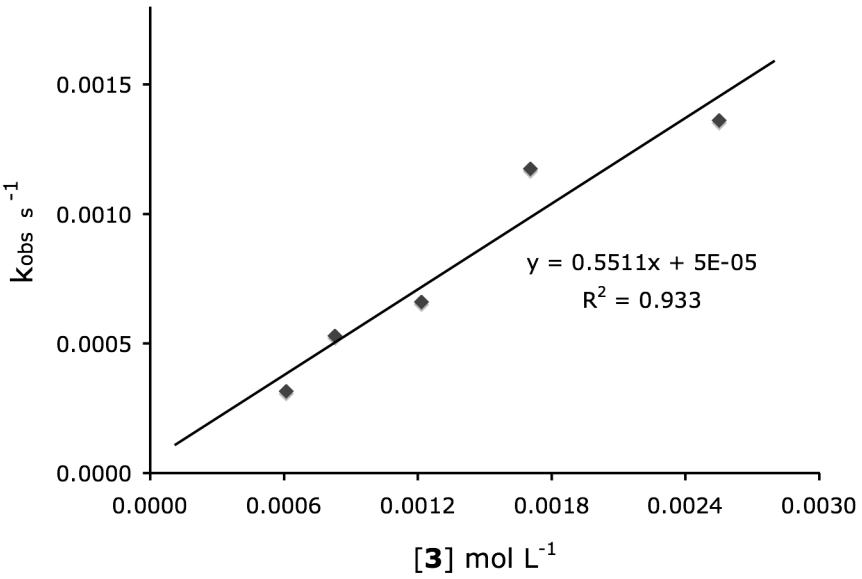

Figure 3.4. Dependence of the observed polymerization rate upon the concentration of **3**.

Table 3.3. Experimental results for polymerization of LA using **3** at various temperatures

Entry	Temperature K	1/T K^{-1}	Ln(k_{obs}/T) mol•$s^{-1}K^{-1}$
1	268.08	0.0037	-14.59
2	278.77	0.0036	-13.88
3	289.79	0.0035	-13.01
4	299.21	0.0033	-12.30
5	305.02	0.0033	-12.02

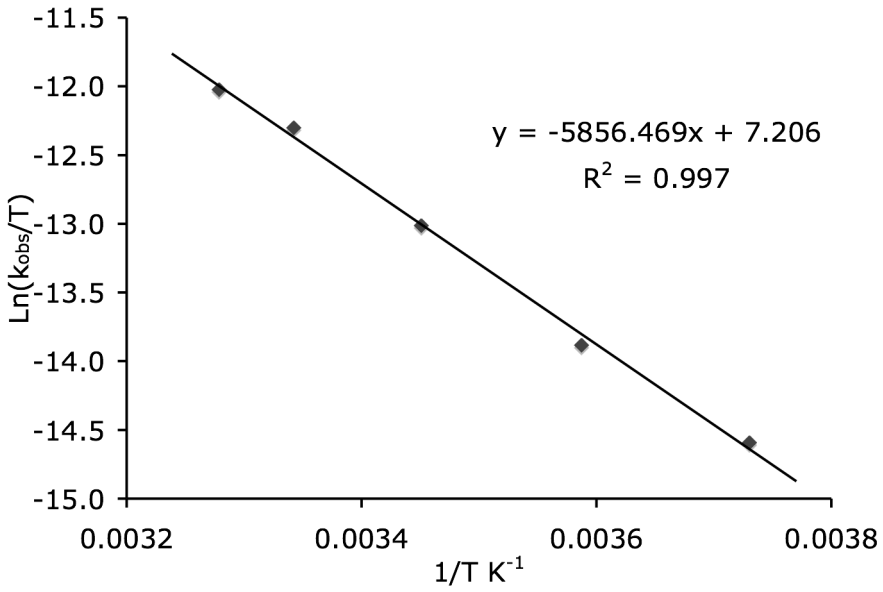

Figure 3.5. Eyring plot for the polymerization of LA using **3**

To elucidate the mechanism of polymerization an Eyring plot was constructed by carrying out a series of polymerizations from -5 to 32 ºC in CD_2Cl_2 (Figure 3.5). When the natural logarithm of the observed rate was plotted versus the inverse of the temperature, the graph was linear. The enthalpy of activation ($\Delta H^{\ddagger}$ = 49(2) kJmol^{-1}) is small while the entropy of activation is large and negative ($\Delta S^{\ddagger}$ = -140(12) JK^{-1}mol^{-1}). These data indicate that the transition state is highly ordered and support an associative coordination insertion mechanism for the polymerization as was proposed previously in literature (Scheme 1.7).

The coordination-insertion mechanism proposes an acyl bond cleavage for the ring-opening polymerization of LA. If the catalysis follows this mechanism then the two ends of the chain should be an alcohol and an ester (upon hydrolysis of the metal complex). If the ethoxide in **7**•LA is acting as the initiator for polymerization an ethyl ester should be observed in the ^{1}H NMR spectrum of the polymer. As seen in Figure 3.6, an ethyl ester is observed at 4.25 ppm in the ^{1}H NMR of an oligomeric sample of PLA ([LA]/[**3**] = 40).

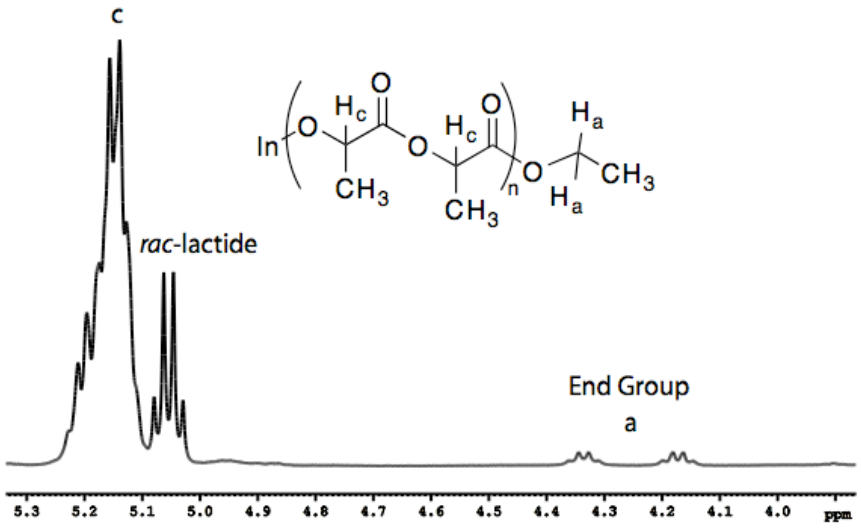

Figure 3.6. ^{1}H NMR spectrum of the methine region of oligomeric PLA (CD_2Cl_2, 298 K, 400MHz)

We propose that **7**•LA initiates the ROP of LA by a coordination-insertion mechanism (Scheme 3.3). After **7**•LA has been formed it can enter into the reaction cycle. The first step is nucleophilic attack by the alkoxide on one of the carbonyl carbons; the data presented so far supports an associative transition state. This is followed by ring-opening of the LA via formation of a new metal-oxygen bond. The new alkoxide (or growing polymer chain) can then continue the cycle upon coordination of another monomer.

Scheme 3.3. Coordination-insertion mechanism for ROP of LA by **7**•LA.

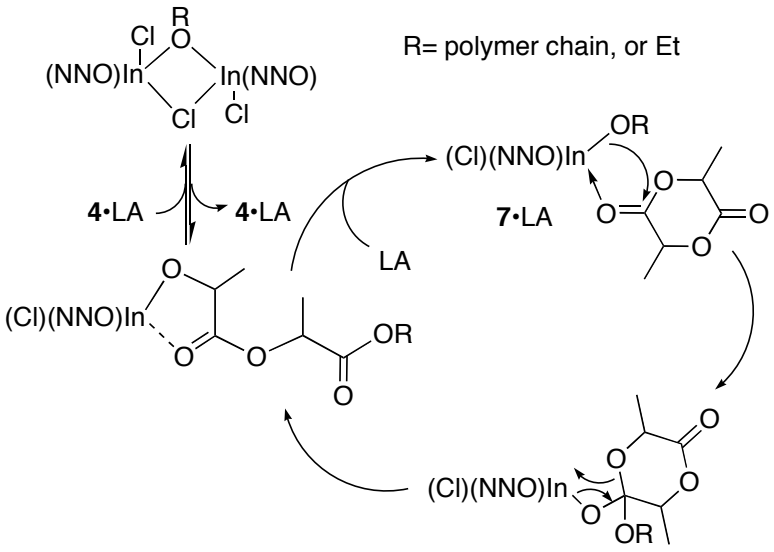

A modification to the general mechanism is required to account for the decay in the observed rate that was noted above 90% conversion for the *in situ* monitoring of ln([LA]/[TMB]) versus time by ^{1}H NMR (Figure 3.3). Since **4**•LA is present in solution it can be postulated that a dinuclear species might reform during the polymerization; **4** would then be competing with LA for coordination sites at the metal. The dinuclear species and the mononuclear species **4**•LA are in an equilibrium that favors the dinuclear species at low [LA] (ie. above 90% conversion). The equilibrium would account for a lower number of active sites being present at higher conversions, leading to a decrease in the rate of polymerization. The dinuclear complex could be considered a resting state for the catalyst; the addition of more lactide causes the equilibrium to shift to favor the lactide adduct which re-enters the catalytic cycle and recommences polymerization. This was demonstrated by the sequential addition of monomer aliquots (Figure 3.3).

A major goal of this research was to develop a stereoselective catalyst for the ROP of LA. In order to determine the stereoselectivity of the catalyst the ^{1}H{^{1}H} and ^{13}C{^{1}H} NMR

spectra were obtained for a series of polymer samples. The temperature, solvents and optical purity of both monomer and catalyst were all varied for this series of polymerizations in the hope that the mechanism for stereocontrol in the polymerization might be elucidated. The $^{1}H\{^{1}H\}$ NMR of the polymer samples reveal a series of peaks corresponding to the mrm, rmr, mmr/rmm, and mmm tetrads (Figure 3.7). The presence of all four peaks in large amounts indicates that the catalyst is not achieving significant stereoselectivity; however, the polymer does show some isotactic enrichment. The relative integration of the mmm tetrad is much larger than it would be for atactic PLA. The ratio of the stereoerror sequences mmr, mrm, rmr, and rmm was found to be roughly 1:2:1:1. As was explained in Section1.5, these values are indicative of enantiomorphic site control mechanism for the stereoselectivity of the catalyst. The methine region of $^{13}C\{^{1}H\}$ NMR spectra of the polymer samples also shows the presence of stereoerror sequences and is consistent with those observed in the $^{1}H\{^{1}H\}$ NMR. The $^{13}C\{^{1}H\}$ NMR confirms a microstructure of isotactically enriched PLA. The peak at 69.4 ppm would have an intensity almost equal to the one observed at 69.2 ppm if the sample was completely atactic.

A polymerization of L-LA was performed using *rac*-**3**, and the $^{1}H\{^{1}H\}$ and $^{13}C\{^{1}H\}$ NMR spectra were obtained (Figure 3.7(c)). The homonuclear decoupled spectrum shows a distinct singlet for the methine region protons of PLA corresponding to the mmm tetrad. Similarly the methine region of the $^{13}C\{^{1}H\}$ NMR spectrum shows one distinct singlet. This is the expected result, as no stereoerror sequences should be formed during the polymerization of enantiopure LA unless racemization of the monomer is occurring.

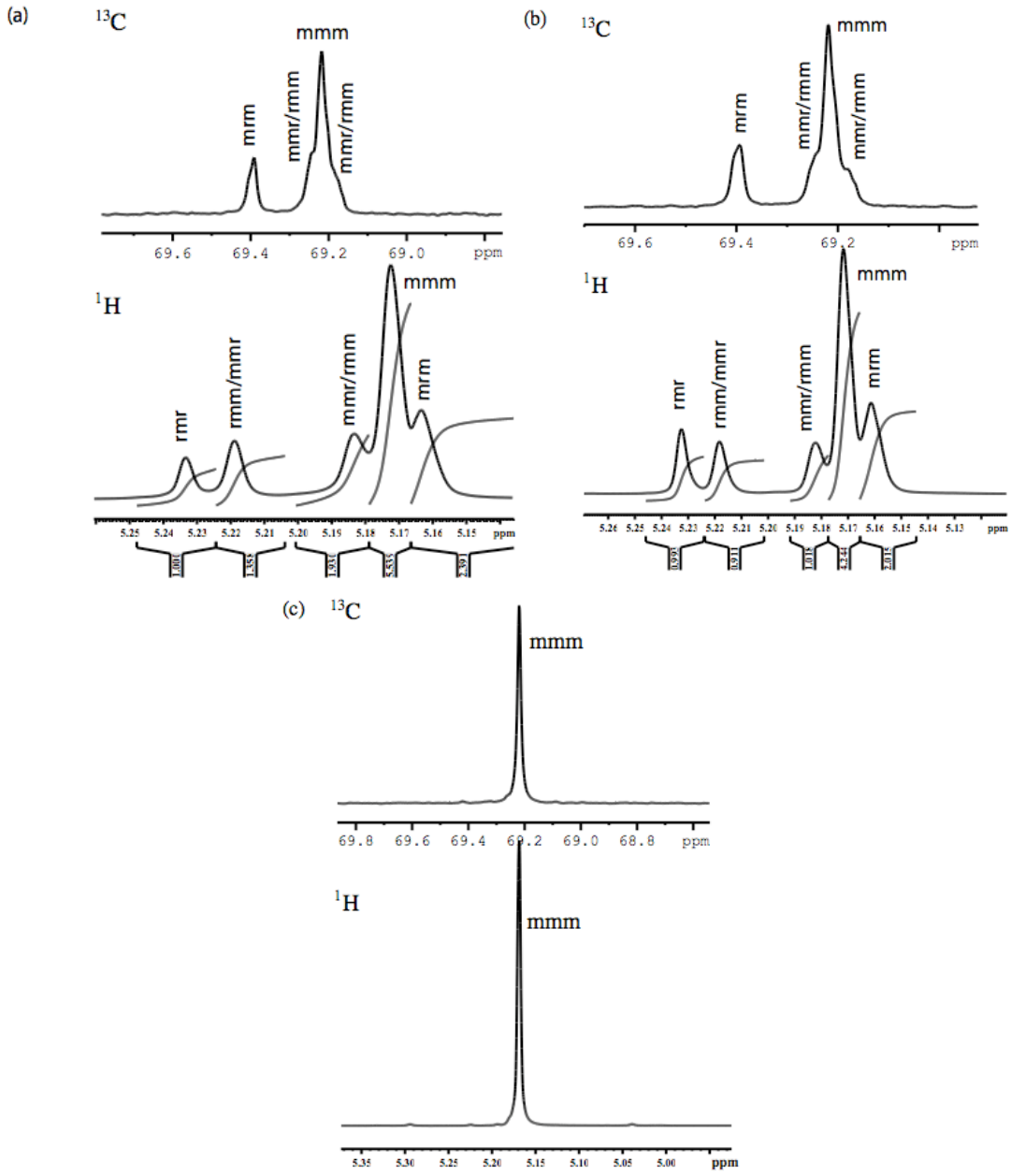

Figure 3.7. $^{1}H\{^{1}H\}$ and $^{13}C\{^{1}H\}$ NMR of PLA ($CDCl_3$, 298 K, 600 MHz) from (a) polymerization of rac-LA using rac-**3** (b) polymerization of rac-LA using RR,RR-**3**, and (c) polymerization of L-LA using rac-**3**.

The relative integration of the stereosequences were also used to calculate the values of P_m and P_r for the catalyst (Table 1.1). The polymerizations were performed in different solvents at room temperature and at 0 ºC (Table 3.4). For a completely random atactic polymer the value

for P_m should be 0.5. All of the polymer samples catalyzed by *rac*-**3** show values of P_m between 0.53 and 0.62 indicating that the polymers are isotactically enriched. The lowest values for P_m corresponds to polymerization carried out in THF, while the highest values are seen for the low temperature experiments.

Table 3.4. P_m and P_r values for polymer samples from the polymerizations of *rac*-LA at 0 ºC and 25 ºC using **3** as a catalyst.

Entry	[LA]/[**3**]	t (h)	Solvent	Temp (°C)	P_m	P_r	$P_r + P_m$
1	205	24	CH_2Cl_2	25	0.59	0.38	0.97
2	200	18	CH_2Cl_2	0	0.62	0.36	0.98
3	200	48	Toluene	25	0.60	0.36	0.96
4	200	48	Toluene	0	0.62	0.34	0.96
5	200	24	THF	25	0.53	0.44	0.97
6[a]	182	18	CH_2Cl_2	25	0.43	0.46	0.89

[a] This sample was prepared with RR,RR-**3**

Results obtained using RR,RR-**3** as the catalyst show very different results. The P_m value (0.43) is significantly lower than that observed for the analogous reaction with *rac*-**3** (0.59), and the P_r value also increased (from 0.38 to 0.46). According to the Bernoullian model the value of $P_r + P_m$ must equal one. If one looks at the $P_r + P_m$ values for entries 1-5 it is clear that the values are all close to one. The value for the sixth entry shows a significant deviation from 1 at 0.89. This indicates that the Bernoullian model has failed for this set of polymerization conditions. Further investigations into the role of the enantiopurity of the catalyst in the polymerization were required to explain this result.

A kinetic study was performed using varying ratios of RR,RR and SS,SS-**3**. A physical mixture of *rac*- and RR,RR-**3** stock solutions was used to control the enantiopurity of the

catalyst. The rates were observed using ^{1}H NMR spectroscopy, and the results are shown in Figure 3.8. As seen in the figure, the rates show a distinctly non-linear behavior with the highest rate being observed for the polymerization of *rac*-LA by *rac*-**3**.

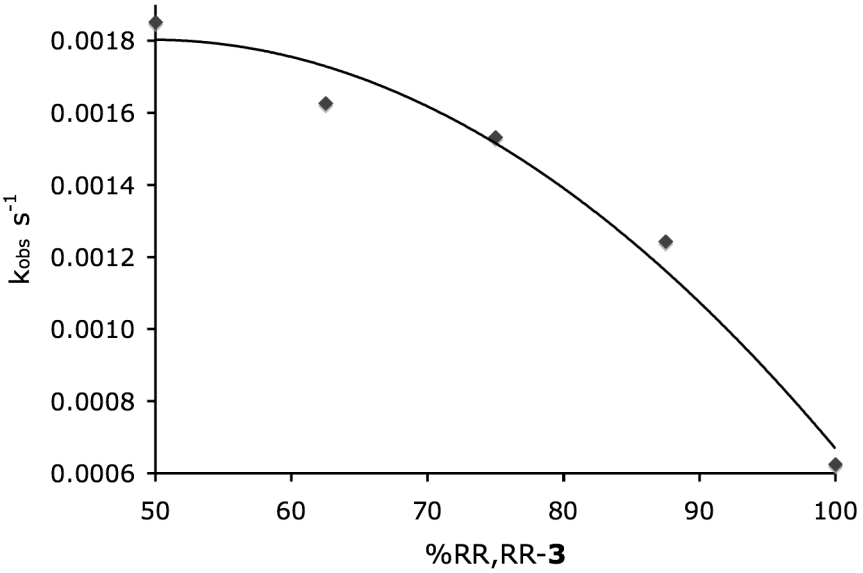

Figure 3.8. The observed rate of polymerization of LA as a function of the enantiomeric composition of the catalyst.

Qualitatively, the variance in rate with enantiopurity of the catalyst is consistent with a site control mechanism. If both enantiomers of a stereoselective catalyst are present in solution then each enantiomer will rapidly polymerize its preferred enantiomer of the monomer. However, as the monomer composition changes from a perfect 50/50 mixture of enantiomers the rate is expected to decrease. A concentration gradient will develop in the mixture; the enantiomer of the catalyst that is in excess (RR,RR-**3**) will deplete its monomer of choice more quickly than the other enantiomer of the catalyst can consumes its enantiomer. As the RR,RR-catalyst runs out of its monomer, the occurrence of stereoerrors in the polymer chain become more frequent and the polymerization slows down.

If the mismatch in chirality of the monomer and catalyst is the cause for the observed decrease in rates then the relative rate for the polymerization of enantiopure LA by RR,RR-**3** should either be much slower than it is for *rac*-LA, or much faster depending if the enantiopure LA is the "right" enantiomer. Therefore, the polymerization of L-LA by RR,RR-**3** was attempted. The observed rate for polymerization of L-LA by RR,RR-**3** was roughly one order of magnitude slower (k_{obs} = 4.4 x 10^{-5} s^{-1}) than the corresponding rate for polymerization of rac-LA by RR,RR-**3** (k_{obs} **=** 2.4 x 10^{-4} s^{-1}) when the same catalyst and monomer concentration is used. This clearly indicates that there is a mismatch between the chirality of the catalyst and that of the monomer. Therefore, it is possible that the RR,RR-**3** enantiomer of the catalyst preferentially polymerizes D-LA, and that the SS,SS-**3** enantiomer of the catalyst prefers L-LA. This assumption could be tested either by synthesizing SS,SS-**3** and testing its rate in the polymerization of L-LA, or by purchasing D-LA and performing the polymerization with RR,RR-**3**.

The above data suggests that the mechanism for stereocontrol exhibited by **3** over the polymerization of LA has a significant component of enantiomorphic site control. However, it is by no means conclusive that chain-end control is not playing a role in the stereoselectivity of the catalyst, as the stereoselectivity is not high enough to obtain strong data (ie P_m values approaching one for isotactic PLA). More selective catalysts must be developed in order to obtain higher stereoselectivity, and control over the polymerization.

3.3 Conclusions and Future Work

Complex rac-**3** has been shown to be a highly active catalyst for the polymerization of LA. The catalyst is more active than previously discovered aluminum-based compounds, although direct comparisons are difficult as there have been no examples of similar tridentate aluminum catalysts for LA ROP reported. Complex **3** is also the first known indium based catalyst for the polymerization of lactide and β-butyrolactone, and the second indium catalyst active for the polymerization for the polymerization of ε-caprolactone.

The system was characterized using a number of techniques including analysis of the isolated polymer samples by GPC and NMR, and by monitoring the reaction kinetics using ^{1}H NMR. The system was living; a linear relationship between molecular weight and monomer loading was observed. The polymer samples obtained from the polymerization had narrow molecular weight distributions. Analysis of the polymer samples by $^{1}H\{^{1}H\}$ and $^{13}C\{^{1}H\}$ NMR spectroscopy showed a degree of isotactic enrichment in the polymer chain. This is attributed to a site-control mechanism due to the chiral nature of the tridentate ligand.

Further investigation into the behaviour of the dinuclear catalyst (**3)** is required. First, a set of kinetic experiments should be performed with varying [**4**]. If the dinuclear species is hindering the catlalytic process either at the early stages during initiation or at low [LA], an overall decrease in the rate of polymerization should be observed with higher [**4**]. Alternatively a similar mononuclear catalyst (of the type L_nInR) should be synthesized; the study of its behaviour in the polymerizations of LA would help to confirm some of the asumptions made about the dinculear system; namely, that the initiation period is due to dissociation of the dinuclear complex.

In order to improve catalyst selectivity a bulkier tridentate chiral catalyst should be

synthesized. Because of the design of the ligand it is relatively facile to change substituents at both the amines as well as the phenol. From the crystal structures of complexes **1** - **6** it can be seen that the indium atom is not very sterically crowded, especially where the dimethylated amine is bound to indium; therefore, we propose to introduce more steric bulk at that location in order to enhance the stereoselectivity of the catalyst. To this end an undergraduate student in our group has synthesized a terminally arylated pro-ligand of H_2NNO (Scheme 3.4). Attempts are currently being made to synthesize an inium catalyst using this pro-ligand.

Scheme 3.4 Possible indium catalysts for the polymerization of LA

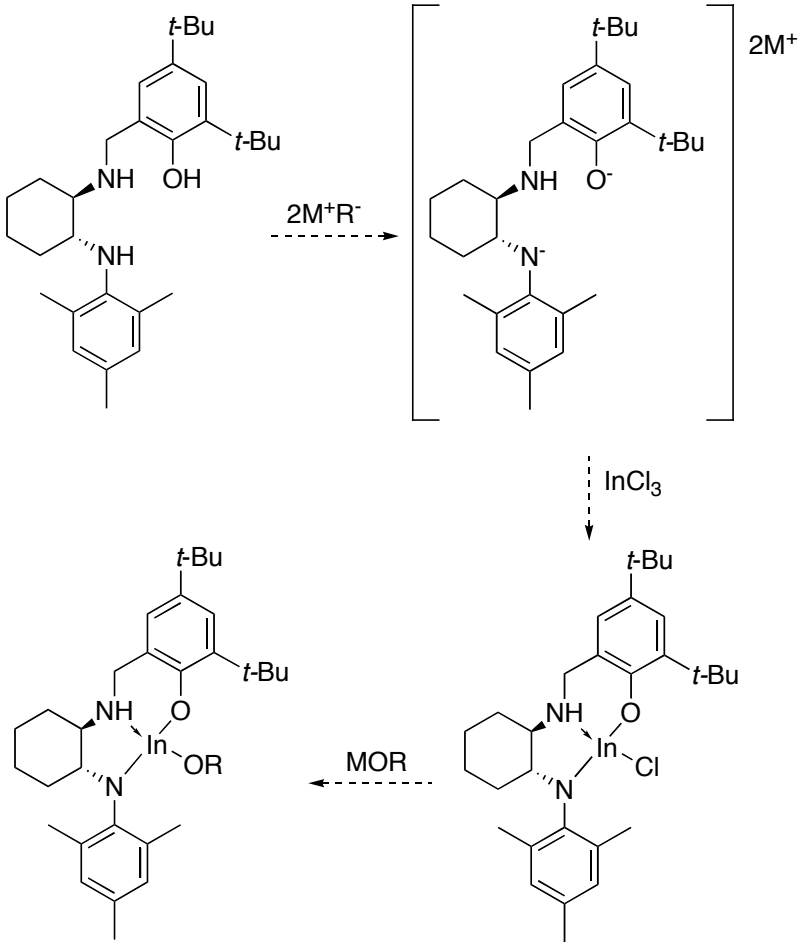

3.4 Experimental

Materials

Solvents (THF, toluene, dichloromethane) were degassed and dried using 3Å molecular sieves in an mBraun Solvent Purification System. The THF was further dried over sodium and distilled under N_2. CD_2Cl_2 and $CDCl_3$ were dried over CaH_2, and degassed through a series of freeze-pump-thaw cycles. DL-lactide and L-lactide was purchased from Alfa Aesar and purified by recrystallization from *iso*-propanol, and toluene. β-butyrolactone and ε-caprolactone were purchased from Aldrich and Alfa Aesar respectively. They were dried over CaH_2, distilled under N_2, and degassed through a series of freeze-pump cycles. 1,3,5-Trimethoxybenzene was purchased from Aldrich and was used without further purification.

General Methods

Unless otherwise indicated, all air- and/or water-sensitive reactions were carried out under dry nitrogen using either an mBraun glovebox or standard Schlenk line techniques. NMR spectra were recorded on either a Bruker Avance 400 MHz or 600 MHz spectrometer. ^{1}H NMR chemical shifts are given in ppm versus residual protons in deuterated solvents as follows: δ 7.27 $CDCl_3$, δ 5.32 CD_2Cl_2. $^{13}C\{^{1}H\}$ NMR chemical shifts are given in ppm versus residual ^{13}C in solvents as follows: δ 77.2 $CDCl_3$. Molecular weights were estimated by triple detection gel permeation chromatography (GPC - LLS) using a Waters liquid chromatograph equipped with a Waters 515 HPLC pump, Waters 717 plus autosampler, Waters Styragel columns (4.6 × 300 mm) HR5E, HR4 and HR2, Waters 2410 differential refractometer, Wyatt tristar miniDAWN (laser light scattering detector) and a Wyatt ViscoStar viscometer. A flow rate of 0.5 mL min^{-1}

was used and samples were dissolved in THF (ca. 1 mg mL^{-1}). Narrow molecular weight polystyrene standards were used for calibration purposes.

NMR scale polymerization of *rac*-lactide with **3**

In a teflon sealed NMR tube, 0.50 mL of **3** in CD_2Cl_2 (0.0048 M, 0.0024 mmol) was added to a solution of *rac*-lactide (66 mg; 0.47 mmol) and 1,3,5-trimethoxybenzene (5 mg; 0.03 mmol) in 0.48 mL of CD_2Cl_2. This mixture was immediately cooled in liquid nitrogen for transport to the instrument. The NMR tube was warmed to room temperature before it was inserted into the instrument (400 MHz Avance Bruker Spectrometer). The polymerization was monitored to ca. 95% conversion.

Large-scale polymerization of *rac*-lactide using **3**

Rac-lactide (129.3 mg, 0.92mmol) was dissolved in 6 mL of CH_2Cl_2 in a vial and stirred using a magnetic stir bar. To this solution 1mL of a stock solution of **3** in CH_2Cl_2 was added (0.0046 M; 0.0046 mmol). The reaction was allowed to proceed for 16 h and then concentrated to dryness. The resulting polymer was dissolved in a minimum amount of CH_2Cl_2 and added to cold wet methanol (0 ºC, 7 mL). The polymer precipitated and was isolated by centrifugation. The supernatant was decanted off and the polymer was dried under high vacuum for 2 hours.

Large-scale polymerizations of β-butyrolactone and ε-caprolactone using **3**.

Butyrolactone (391 mg, 4.5 mmol) was dissolved in 6 mL of THF in a vial and stirred using a magnetic stir bar. To this solution 1mL of **3** in THF was added (10 mg; 0.01 mmol). The reaction was allowed to proceed at room temperature for 16 h and then concentrated to dryness. The resulting polymer was dissolved in a minimum amount of CH_2Cl_2 and added to cold wet methanol (0 ºC, 15 mL). The polymer precipitated and was isolated by centrifugation. The

supernatant was decanted off and the polymer was dried under high vacuum for 2 hours. Similar conditions were used for the polymerization of ε-caprolactone by **3**.

BIBLIOGRAPHY

1. Drumright, R. E., Gruber, P. R.,Henton, D. E., *Adv. Mater.* **2000,** 12, 1841-1846.
2. Gupta, B., Revagade, N.,Hilborn, J., *Prog. Polym. Sci.* **2007,** 32, 455.
3. Masaki, K., Kamini, N. R., Ikeda, H.,Iefuji, H., *Appl. Environ. Microbiol.* **2005,** 71, 7548-7550.
4. Reeve, M. S., McCarthy, S. P., Downey, M. J.,Gross, R. A., *Macromolecules* **1994,** 27, 825-831.
5. McNaught, A. D.,Wilkinson, A., *Compendium of chemical terminoloy: IUPAC recommendations*. Blackwell Science: Oxford, 1997.
6. Kricheldorf, H. R.,Kreiser-Saunders, I., *Makromol. Chem.* **1990,** 191, 1057-66.
7. Dubois, P., Jacobs, C., Jerome, R.,Teyssie, P., *Macromolecules* **1991,** 24, 2266-70.
8. Culkin, D. A., Jeong, W., Csihony, S., Gomez, E. D., Balsara, N. P., Hedrick, J. L.,Waymouth, R. M., *Angew. Chem., Int. Ed.* **2007,** 46, 2627-2630.
9. Dechy-Cabaret, O., Martin-Vaca, B.,Bourissou, D., *Chem. Rev.* **2004,** 104, 6147-6176.
10. Van Hummel, G. J., Harkema, S., Kohn, F. E.,Feijen, J., *Acta Crystallogr., Sect. B* **1982,** B38, 1679-81.
11. Duda, A.,Penczek, S., *Macromolecules* **1990,** 23, 1636-1639.
12. Numata, K., Srivastava, R. K., Finne-Wistrand, A., Albertsson, A. C., Doi, Y.,Abe, H., *Biomacromolecules* **2007,** 8, 3115-3125.
13. Shuichi Matsumura, K. M. K. T., *Macromol. Rapid Commun.* **1997,** 18, 477-482.
14. Dong, H., Wang, H.-D., Cao, S.-G.,Shen, J.-C., *Biotechnol. Lett.* **1998,** 20, 905-908.
15. Kasperczyk, J. E., *Macromolecules* **1995,** 28, 3937-3939.
16. Kricheldorf, H. R.,Dunsing, R., *Makromol. Chem.* **1986,** 187, 1611-25.

17. Kricheldorf, H. R.,Kreiser, I., *Makromol. Chem.* **1987,** 188, 1861-73.

18. Lou, X., Detrembleur, C.,Jerome, R., *Macromolecules* **2002,** 35, 1190-1195.

19. Shibasaki, Y., Sanada, H., Yokoi, M., Sanda, F.,Endo, T., *Macromolecules* **2000,** 33, 4316-4320.

20. Bourissou, D., Martin-Vaca, B., Dumitrescu, A., Graullier, M.,Lacombe, F., *Macromolecules* **2005,** 38, 9993-9998.

21. Pratt, R. C., Lohmeijer, B. G. G., Long, D. A., Waymouth, R. M.,Hedrick, J. L., *J. Am. Chem. Soc.* **2006,** 128, 4556-4557.

22. Csihony, S., Culkin, D. A., Sentman, A. C., Dove, A. P., Waymouth, R. M.,Hedrick, J. L., *J. Am. Chem. Soc.* **2005,** 127, 9079-9084.

23. Dove, A. P., Li, H., Pratt, R. C., Lohmeijer, B. G. G., Culkin, D. A., Waymouth, R. M.,Hedrick, J. L., *Chem. Commun.* **2006**, 2881-2883.

24. Fredrik Nederberg, E. F. C. M. M. T. G. J. L. H., *Angew. Chem. Int. Ed.* **2001,** 40, 2712-2715.

25. Chamberlain, B. M., Cheng, M., Moore, D. R., Ovitt, T. M., Lobkovsky, E. B.,Coates, G. W., *J. Am. Chem. Soc.* **2001,** 123, 3229-3238.

26. Chisholm, M. H., Eilerts, N. W., Huffman, J. C., Iyer, S. S., Pacold, M.,Phomphrai, K., *J. Am. Chem. Soc.* **2000,** 122, 11845-11854.

27. Tang, H.-Y., Chen, H.-Y., Huang, J.-H.,Lin, C.-C., *Macromolecules* **2007,** 40, 8855-8860.

28. Chisholm, M. H., Gallucci, J.,Phomphrai, K., *Chem. Commun.* **2003**, 48-49.

29. Chisholm, M. H., Gallucci, J. C.,Phomphrai, K., *Inorg. Chem.* **2005,** 44, 8004-8010.

30. Lian, B., Thomas, C. M., Casagrande, O. L., Jr., Roisnel, T.,Carpentier, J.-F., *Polyhedron* **2007,** 26, 3817-3824.

31. Wu, J.-C., Huang, B.-H., Hsueh, M.-L., Lai, S.-L.,Lin, C.-C., *Polymer* **2005,** 46, 9784-9792.

32. Ejfler, J., Kobylka, M., Jerzykiewicz, L. B.,Sobota, P., *Dalton Trans.* **2005**, 2047-2050.

33. Chivers, T., Fedorchuk, C.,Parvez, M., *Organometallics* **2005,** 24, 580-586.

34. Chisholm, M. H., Gallucci, J. C.,Phomphrai, K., *Inorg. Chem.* **2004,** 43, 6717-25.

35. Chen, H.-Y., Tang, H.-Y.,Lin, C.-C., *Polymer* **2007,** 48, 2257-2262.

36. Chisholm, M. H., Gallucci, J. C.,Phomphrai, K., *Inorg. Chem.* **2004,** 43, 6717-6725.

37. Zhong, Z., Schneiderbauer, S., Dijkstra, P. J., Westerhausen, M.,Feijen, J., *Polym. Bull.* **2003,** 51, 175-182.

38. Abderramane Amgoune, C. M. T. S. I. T. R. J.-F. C., *Angew. Chem. Int. Ed.* **2006,** 45, 2782-2784.

39. Abderramane Amgoune, C. M. T. J.-F. C., *Macromol. Rapid Commun.* **2007,** 28, 693-697.

40. Ovitt, T. M.,Coates, G. W., *J. Am. Chem. Soc.* **2002,** 124, 1316-1326.

41. Liu, X., Shang, X., Tang, T., Hu, N., Pei, F., Cui, D., Chen, X.,Jing, X., *Organometallics* **2007,** 26, 2747-2757.

42. Cai, C.-X., Amgoune, A., Lehmann, C. W.,Carpentier, J.-F., *Chem. Commun.* **2004**, 330-331.

43. Shang, X., Liu, X.,Cui, D., *J. Polym. Sci., Part A: Polym. Chem.* **2007,** 45, 5662-5672.

44. Miao, W., Li, S., Zhang, H., Cui, D., Wang, Y.,Huang, B., *J. Organomet. Chem.* **2007,** 692, 4828-4834.

45. Platel, R. H., Hodgson, L. M., White, A. J. P.,Williams, C. K., *Organometallics* **2007,** 26, 4955-4963.

46. Yang, Y., Li, S., Cui, D., Chen, X.,Jing, X., *Organometallics* **2007,** 26, 671-678.

47. Hodgson, L. M., White, A. J. P.,Williams, C. K., *J. Polym. Sci., Part A: Polym. Chem.* **2006,** 44, 6646-6651.

48. Alaaeddine, A., Amgoune, A., Thomas, C. M., Dagorne, S., Bellemin-Laponnaz, S.,Carpentier, J.-F., *Eur. J. Inorg. Chem.* **2006**, 3652-3658.

49. Westmoreland, I.,Arnold, J., *Dalton Trans.* **2006**, 4155-4163.

50. Skvortsov, G. G., Yakovenko, M. V., Castro, P. M., Fukin, G. K., Cherkasov, A. V., Carpentier, J.-F.,Trifonov, A. A., *Eur. J. Inorg. Chem.* **2007**, 3260-3267.

51. Miao, W., Li, S., Cui, D.,Huang, B., *J. Organomet. Chem.* **2007,** 692, 3823-3834.

52. Heck, R., Schulz, E., Collin, J.,Carpentier, J.-F., *J. Mol. Catal. A: Chem.* **2007,** 268, 163-168.

53. Amgoune, A., Thomas, C. M., Roisnel, T.,Carpentier, J.-F., *Chem. Eur. J.* **2005,** 12, 169-179.

54. Ma, H., Spaniol, T. P.,Okuda, J., *Dalton Trans.* **2003**, 4770-4780.

55. O'Keefe, B. J., Hillmyer, M. A.,Tolman, W. B., *J. Chem. Soc., Dalton Trans.* **2001**, 2215-2224.

56. Haiyan Ma, T. P. S. J. O., *Angew. Chem. Int. Ed.* **2006,** 45, 7818-7821.

57. Dove, A. P., Gibson, V. C., Marshall, E. L., Rzepa, H. S., White, A. J. P.,Williams, D. J., *J. Am. Chem. Soc.* **2006,** 128, 9834-9843.

58. Kowalski, A., Libiszowski, J., Biela, T., Cypryk, M., Duda, A.,Penczek, S., *Macromolecules* **2005,** 38, 8170-8176.

59. Nimitsiriwat, N., Marshall, E. L., Gibson, V. C., Elsegood, M. R. J.,Dale, S. H., *J. Am. Chem. Soc.* **2004,** 126, 13598-13599.

60. Lahcini, M., Castro, P. M., Kalmi, M., Leskelae, M.,Repo, T., *Organometallics* **2004,** 23, 4547-4549.

61. Wang, X., Liao, K., Quan, D.,Wu, Q., *Macromolecules* **2005,** 38, 4611-4617.

62. McGuinness, D. S., Marshall, E. L., Gibson, V. C.,Steed, J. W., *J. Polym. Sci., Part A: Polym. Chem.* **2003,** 41, 3798-3803.

63. Gibson, V. C., Marshall, E. L., Navarro-Llobet, D., White, A. J. P.,Williams, D. J., *J. Chem. Soc., Dalton Trans.* **2002**, 4321-4322.

64. O'Keefe, B. J., Monnier, S. M., Hillmyer, M. A.,Tolman, W. B., *J. Am. Chem. Soc.* **2001,** 123, 339-340.

65. Williams, C. K., Breyfogle, L. E., Choi, S. K., Nam, W., Young, V. G., Hillmyer, M. A.,Tolman, W. B., *J. Am. Chem. Soc.* **2003,** 125, 11350-11359.

66. Hormnirun, P., Marshall, E. L., Gibson, V. C., White, A. J. P.,Williams, D. J., *J. Am. Chem. Soc.* **2004,** 126, 2688-2689.

67. Zhong, Z., Dijkstra, P. J.,Feijen, J., *J. Am. Chem. Soc.* **2003,** 125, 11291-11298.

68. Emig, N., Nguyen, H., Krautscheid, H., Reau, R., Cazaux, J. B.,Bertrand, G., *Organometallics* **1998,** 17, 3599-3608.

69. Hormnirun, P., Marshall, E. L., Gibson, V. C., Pugh, R. I.,White, A. J. P., *Proc. Natl. Acad. Sci. U. S. A.* **2006,** 103, 15343-15348.

70. Ovitt, T. M.,Coates, G. W., *J. Polym. Sci., Part A: Polym. Chem.* **2000,** 38, 4686-4692.

71. Trofimoff, L., Aida, T.,Inoue, S., *Chem. Lett.* **1987**, 991-4.

72. Radano, C. P., Baker, G. L.,Smith, M. R., III, *J. Am. Chem. Soc.* **2000,** 122, 1552-1553.

73. Zhong, Z., Dijkstra, P. J.,Feijen, J., *Angew. Chem., Int. Ed.* **2002,** 41, 4510-4513.

74. Nomura, N., Ishii, R., Yamamoto, Y.,Kondo, T., *Chem. Eur. J.* **2007,** 13, 4433-4451.

75. Chmura, A. J., Chuck, C. J., Davidson, M. G., Jones, M. D., Lunn, M. D., Bull, S. D.,Mahon, M. F., *Angew. Chem., Int. Ed.* **2007,** 46, 2280-2283.

76. Finne, A., Reema,Albertsson, A.-C., *J. Polym. Sci., Part A: Polym. Chem.* **2003,** 41, 3074-3082.

77. Kowalski, A., Duda, A.,Penczek, S., *Macromolecules* **2000,** 33, 7359-7370.

78. Stevels, W. M., Ankone, M. J. K., Dijkstra, P. J.,Feijen, J., *Macromolecules* **1996,** 29, 6132-6138.

79. Stevels, W. M., Ankone, M. J. K., Dijkstra, P. J.,Feijen, J., *Macromolecules* **1996,** 29, 3332-3.

80. Zhong, Z., Dijkstra, P. J., Birg, C., Westerhausen, M.,Feijen, J., *Macromolecules* **2001,** 34, 3863-3868.

81. Hans R. Kricheldorf, M. B., Nico Scharnagl, *Macromolecules* **1988,** 21, 286-293.

82. Aida, T.,Inoue, S., *Acc. Chem. Res.* **1996,** 29, 39-48.

83. Emig, N., Reau, R., Krautscheid, H., Fenske, D.,Bertrand, G., *J. Am. Chem. Soc.* **1996,** 118, 5822-5823.

84. Dumitrescu, A., Martin-Vaca, B., Gornitzka, H., Cazaux, J.-B., Bourissou, D.,Bertrand, G., *Eur. J. Inorg. Chem.* **2002**, 1948-1951.

85. Faure, J.-L., Gornitzka, H., Reau, R., Stalke, D.,Bertrand, G., *Eur. J. Inorg. Chem.* **1999**, 2295-2299.

86. Chisholm, M. H., Patmore, N. J.,Zhou, Z., *Chem. Commun.* **2005**, 127-129.

87. Agustin, D., Rima, G., Gornitzka, H.,Barrau, J., *J. Organomet. Chem.* **1999,** 592, 1-10.

88. Thakur, S. S., Chen, S.-W., Li, W., Shin, C.-K., Kim, S.-J., Koo, Y.-M.,Kim, G.-J., *J. Organomet. Chem.* **2006,** 691, 1862.

89. Chisholm Malcolm, H., Gallucci, J.,Phomphrai, K., *Inorg. Chem.* **2002,** 41, 2785-94.

90. Chisholm, M. H., Huffman, J. C.,Phomphrai, K., *J. Chem. Soc., Dalton Trans.* **2001**, 222-224.

91. Dove, A. P., Gibson, V. C., Marshall, E. L., White, A. J. P.,Williams, D. J., *Chem. Commun.* **2001**, 283-284.

92. Cheng, M., Attygalle, A. B., Lobkovsky, E. B.,Coates, G. W., *J. Am. Chem. Soc.* **1999,** 121, 11583-11584.

93. Natta, G., Pino, P., Corradini, P., Danusso, F., Mantica, E., Mazzanti, G.,Moraglio, G., *J. Am. Chem. Soc.* **1955,** 77, 1708-1710.

94. Bovey, F. A.,Mirau, P. A., *NMR of Polymers.* Academic Press: San Diego, 1996.

95. Ovitt, T. M.,Coates, G. W., *J. Am. Chem. Soc.* **1999,** 121, 4072-4073.

96. Russell, S. K., Gamble, C. L., Gibbins, K. J., Juhl, K. C. S., Mitchell, W. S., III, Tumas, A. J.,Hofmeister, G. E., *Macromolecules* **2005,** 38, 10336-10340.

97. Greenwood, N. N.,Earnshaw, A., *Chemistry of the Elements. 2nd Ed.* Butterworth-Heinemann: Boston, 1997.

98. Carlin, J. F. J., Mineral Commodities Studies: Indium. In U.S. Geological Survey: 2006; pp 82-83.

99. Fringuelli, F., Piermatti, O., Pizzo, F.,Vaccaro, L., *Curr. Org. Chem.* **2003,** 7, 1661.

100. Loh, T.-P.,Chua, G.-L., *Chem. Commun.* **2006**, 2739-2749.

101. Teo, Y. C.,Loh, T. P., *Org. Lett.* **2005,** 7, 2539-2541.

102. Kamlesh K. Chauhan, C. G. F., *J. Chem. Soc., Perkin Trans. 1* **2000**, 3015-3019.

103. Hsieh, I. P., Huang, C.-H., Lee, H. M., Kuo, P.-C., Huang, J.-H., Lee, H.-I., Cheng, J.-T.,Lee, G.-H., *Inorg. Chim. Acta* **2006,** 359, 497.

104. Douglas, A., F., Patrick, B., O.,Mehrkhodavandi, P., *Angew. Chem. Int. Ed. Engl.* **2008,** 47, 2290-3.

105. Mitchell, J. M.,Finney, N. S., *Tetrahedron Lett.* **2000,** 41, 8431.

106. Xu, C., Baum, T. H., Guzei, I.,Rheingold, A. L., *Inorg. Chem.* **2000,** 39, 2008-2010.

107. Chou, T.-Y., Chi, Y., Huang, S.-F., Liu, C.-S., Carty, A. J., Scoles, L.,Udachin, K. A., *Inorg. Chem.* **2003,** 42, 6041-6049.

108. Lewinski, J., Zachara, J.,Starowieyski, K. B., *J. Chem. Soc., Dalton Trans.* **1997**, 4217-4222.

109. Schumann, H., Kaufmann, J.,Dechert, S., *Z. Anorg. Allg. Chem.* **2004,** 630, 1999-2005.

110. Suh, S.,Hoffman, D. M., *J. Am. Chem. Soc.* **2000,** 122, 9396-9404.

111. Kim, J., Bott, S. G.,Hoffman, D. M., *Inorg. Chem.* **1998,** 37, 3835-3841.

112. Sussek, H., Stark, O., Devi, A., Pritzkow, H.,Fischer, R. A., *J. Organomet. Chem.* **2000,** 602, 29.

113. Lin, Z., Jiang, F., Chen, L., Yuan, D.,Hong, M., *Inorg. Chem.* **2005,** 44, 73-6.

114. Zhou, Y.,Richeson, D. S., *Organometallics* **1995,** 14, 3558-61.

115. Stender, M., Eichler, B. E., Hardman, N. J., Power, P. P., Prust, J., Noltemeyer, M.,Roesky, H. W., *Inorg. Chem.* **2001,** 40, 2794-9.

116. Eric N. Jacobsen, W. Z., Alexander R. Muci, James R. Ecker, Li Deng, *J. Am. Chem. Soc.* **1991,** 113, 7063-7064.

117. Holm, T., *Tetrahedron Lett.* **1966**, 3329-36.

118. Burger, H., Cichon, J., Goetze, U., Wannagat, U.,Wismar, H. J., *J. Organomet. Chem.* **1971,** 33, 1.

119. Evans pKa Table. http://www2.lsdiv.harvard.edu/labs/evans/pdf/evans_pKa_table.pdf

120. Schlosser, M., *Organometallics in Synthesis: A Manual, 2nd ed.* Wiley: Chichester, 2002; p 292.

121. Schlosser, M.,Hartmann, J., *Angew. Chem.* **1973,** 85, 544-5.

122. Atkins, P.,de Paula, J., *Physical Chemistry, 7th ed.* W.H. Freeman and Company: New York, 2002.

123. Berger, S.,Siegmar, B., *200 and More NMR Experiments: A Practical Course*. WILEY-VCH: Weinham, **2004**; p 141-148.

124. Skoog, D. A.,Holler, J. F., *Principles of Instrumental Analysis, 5th ed*. Nelson Thomson Learning: Toronto, 1998.

APPENDIX 1

X-Ray Crystallography Data

Table A.1. Selected crystal structure data for **1**, **2**, and **3**

	1	**2**	**3**
Formula	$C_{25}H_{45}N_2OIn$	$C_{29.5}H_{57}N_2OIn_2Cl$	$C_{62}H_{97}N_4O_3In_2Cl_3$
mol wt	504.45	720.86	1282.43
Crystal System	orthorhombic	monoclinic	monoclinic
Space Group	*P bca*	*C* 2/*c*	$P\,2_1/c$
a/Å	19.6863(12)	20.904(3)	16.905(2)
b/Å	13.1562(8)	13.314(2)	20.967(2)
c/Å	20.1573(10)	25.413(5)	18.428(1)
α/°	90	90	90
β/Å	90	111.765(9)	94.020(4)
γ/°	90	90	90
V/Å^3	5220.68(5)	6569(2)	6515(1)
ρ_{calc}/g cm^{-3}	1.284	1.458	1.307
Z	8	8	4
μ (Mo-Kα) / mm^{-1}	9.22	15.08	8.74
Reflection Collected/ Unique (R_{int})	80087/6271 (0.059)	38177/8249 (0.05)	42181/8470 (0.062)
Residuals (refined on F2, all data): R1; wR2	0.049; 0.062	0.073; 0.106	0.122; 0.181
Residuals (refined on F): R1; wR2	0.027; 0.054	0.045; 0.095	0.081; 0.168

Table A.2. Selected crystal data for **4**•Py, **5**, and **6**

	4•Py	**5**	**6**
Formula	$C_{35}H_{52}N_3OInCl_2$	$C_{59}H_{86}N_6O_4In_2Cl_2$	$C_{61}H_{93}N_4O_3In_2Cl_3$
mol wt	716.52	1135.79	1266.38
Crystal System	monoclinic	primitive	triclinic
Space Group	$P2_1/c$	P-1	P-1
a/Å	11.2696(11)	8.5090(8)	11.5642(5)
b/Å	20.749(2)	9.6905(9)	16.8754(8)
c/Å	15.4251(14)	16.916(2)	18.1223(8)
a/^{o}	90	87.023(6)	92.263(2)
b/Å	100.875(5)	88.076(6)	106.473(2)
g/^{o}	90	89.371(6)	109.942(2)
V/Å^3	3542.0(6)	1392.1(2)	3151.5(2)
r_{calc}/g cm^{-3}	1.344	1.355	1.335
Z	4	1	2
m (Mo-Ka) / mm^{-1}	8.48	9.69	9.03
Reflection Collected/ Unique (R_{int})	38088/8462 (0.021)	14217/4962 (0.044)	48876/11134 (0.048)
Residuals (refined on F2, all data): R1; wR2	0.026; 0.050	0.079; 0.164	0.065; 0.063
Residuals (refined on F): R1; wR2	0.020; 0.047	0.070; 0.159	0.034; 0.055